

**Continuous Transverse
Excitation for Measuring Chromaticity from the
Head-Tail Phase Difference: An Analytic
Approximation with Experimental
Data**

Cheng-Yang Tan
Vahid Ranjbar

Accelerator Division/Tevatron

ABSTRACT: We will explore a method for measuring chromaticity by continuously kicking the beam transversely. This is called the continuous head-tail method for measuring chromaticity. The complete analytic approximation in terms of trigonometric functions is derived for zero transverse emittance beam. A few examples are used to compare this solution with numerical ones and they are found to be nearly identical. A simple formula for calculating chromaticity from experimental data is also shown. Finally the theory is compared with experimental data.

INTRODUCTION

Continuous chromaticity control up the ramp and through the squeeze will be vital for operating the Large Hadron Collider (LHC). It is especially important at the beginning of the ramp because of snapback where chromaticity swings are expected to drift at a rate of 0.33 s^{-1} even with pre-programmed chromaticity correction tables. This is to be compared to the tolerance required for nominal 7 TeV head-on collisions operations which is ± 1 unit.¹ It is because of these tight tolerances that a chromaticity feedback system has been envisioned for the LHC. However, the best method for measuring chromaticity which has a measurement rate of about 1 Hz has not yet been pinned down. During the 2006 Tune Feedback Review 2006, it was pointed out that there are at least five different methods for doing this.² One method, however, stirred up considerable interest: the continuous head-tail measurement technique.

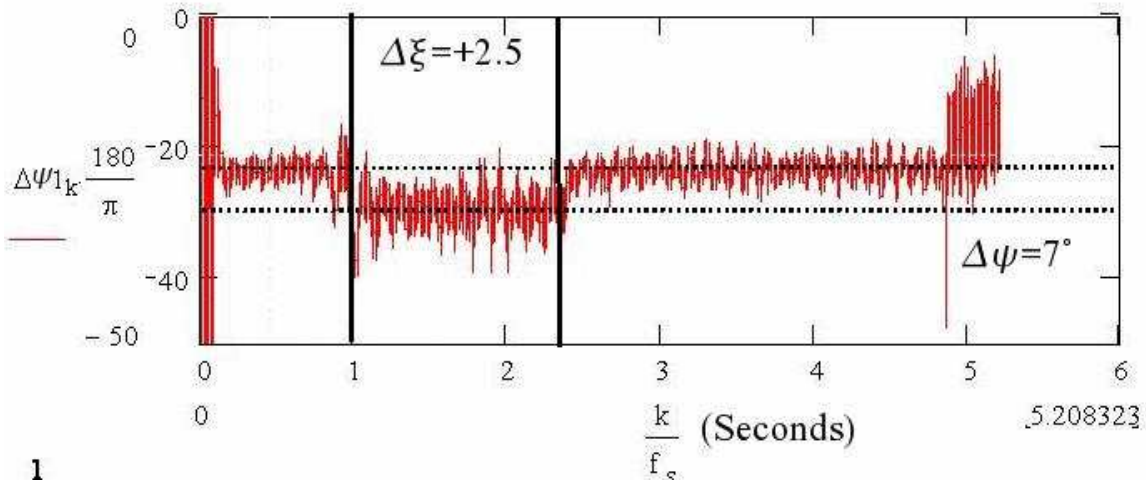


Figure 1 The phase difference between the head and tail with continuous kicks was measured by M. Gasior in the SPS during the machine studies period on 29 Sep 2006. The data were analysed by V. Ranjbar. This showed that the head-tail phase changed when the chromaticity was increased by 2.5 units.

To start off the discussion, we will look first at the traditional head-tail method. In this method, the beam is kicked once transversely and because of chromaticity, the head and the tail de-phase differently.³ When the phase difference between the head and the tail is measured, it can be shown that when the phases are maximally different, this difference is linearly related to the chromaticity. However, this technique although proven to work at both CERN and Fermilab, suffers from at least three deficiencies:

- (i) It causes large emittance growth because of the large kicks.
- (ii) The chromaticity cannot be continuously measured because after a small number of kicks (< 5), there is so much beam loss that the S/N becomes really poor.
- (iii) It is not compatible with the phase locked loop (PLL) tune tracking method.

The first time that we had heard of the continuous head-tail method was in early 2006.⁴ Some preliminary measurements at the Relativistic Heavy Ion Collider (RHIC) have shown a phase difference between the head and the tail which changed with chromaticity. Later work at the Super Proton Synchrotron (SPS) also measured a phase difference. See Figure 1. However, careful examination of the data revealed that only a few data sets showed this correlation. These results begged a theoretical understanding of whether the phase difference was real or not. If this method can be proven to work it has the following advantages:

- (i) There is already a continuous transverse kick from the tune tracker PLL. It has already been demonstrated at Fermilab, RHIC, and SPS that these small kicks $\ll 1 \mu\text{m}$ do not blow up the emittance or cause beam lifetime problems.
- (ii) No extra modulations are required for the chromaticity measurement. For example, the traditional method for measuring chromaticity requires changing the RF frequency to change the momentum of the beam.
- (iii) It is compatible with the tune tracker PLL.

Therefore, the goal of this paper is to answer the following two questions:

- (i) Is there a phase difference between the head and tail when the bunch is continuously kicked transversely?
- (ii) Is there a formula which connects chromaticity to this phase difference if (i) is true?

We will answer these questions with theory, computer simulations and experiment. Note that many of the following pages are filled with mathematical verbiage that can be skipped. For the convenience of the reader, we have boxed the more important mathematical results.

Theory

THEORY

Most of this paper consists of our attempts at arriving at an analytic solution for the phase difference between the head and the tail of the bunch. In order to assist the reader in navigating this morass, we have plotted a roadmap that should assist him in this long and arduous journey. We must point out that many of the mathematical details can be skipped and for convenience, we have boxed the more important results of each section. The roadmap is:

- (i) We write down the ordinary differential equation (o.d.e.) which describes the dynamics of a single particle.
- (ii) We transform to a rotating frame which simplifies the o.d.e. In this frame, we find that it is a simple harmonic oscillator with two forcing terms: one from the transverse kick of the tune tracker PLL and the other from the radio frequency (RF) (which is the source of the synchrotron frequency).
- (iii) The Method of Averaging is used to solve the o.d.e. for two cases: (a) when the transverse kick is on the betatron frequency and (b) when the transverse kick is close to the betatron frequency.
- (iv) The solution in the rotating frame is transformed back to the laboratory frame.
- (v) The phase difference between the head and tail is calculated.
- (vi) The particles in phase space are projected down from momentum space onto position space so as to reflect what is seen from the output of the beam position monitors.

At every step along the way, we will try to verify the approximate solutions with numerically integrated solutions of the o.d.e. This will at least give us some confidence that the results are (maybe) correct.

The Differential Equation

We can write down the transverse equation of motion for a single particle as

$$\frac{d^2 X(s)}{ds^2} + \frac{\omega_Q^2}{c^2} X(s) = 0 \quad (1)$$

Here X is the transverse position of the particles, s is the longitudinal coordinate and ω_Q is the betatron frequency and c is the speed of light. However, if the particle resides in an RF-bucket, we must consider its longitudinal motion inside the bucket and so the equation of motion becomes

$$\frac{d^2 X(s, \delta, z)}{ds^2} + \frac{\omega_Q^2(\delta)}{c^2} X(s, \delta, z) = 0 \quad (2)$$

Here z defines the longitudinal position relative to the centre of the RF-bucket and δ is the relative momentum difference from the “on momentum” particle. If we expand the betatron frequency to first order in δ we obtain

$$\omega_Q(\delta) = \omega_0 Q + \xi \omega_0 \delta \quad (3)$$

where ω_0 is the revolution frequency, $Q = \omega_Q/\omega_0$ is the betatron tune and ξ is the chromaticity. Therefore (2) becomes

$$\frac{d^2 X(s, \delta, z)}{ds^2} + \omega_0^2 (Q + \xi \delta)^2 X(s, \delta, z) = 0 \quad (4)$$

We will approximate the longitudinal motion inside the RF-bucket with

$$\left. \begin{aligned} \delta(s) &= -\frac{\omega_s}{\eta c} r \sin\left(\frac{\omega_s s}{c} + \phi\right) \\ z(s) &= r \cos\left(\frac{\omega_s s}{c} + \phi\right) \end{aligned} \right\} \quad (5)$$

where ω_s is the synchrotron frequency, (r, ϕ) is position of the particle at $s/c = 0$ and η is the slip factor. See Figure 2. It is clear from this figure, that we can write down a linear transformation which maps $(z(0), \delta(0)) \equiv (z_0, \delta_0)$ to $(z(s), \delta(s))$

$$\begin{pmatrix} z(s) \\ \delta(s) \end{pmatrix} = \begin{pmatrix} \cos\left(\frac{\omega_s s}{c}\right) & \frac{\eta c}{\omega_s} \sin\left(\frac{\omega_s s}{c}\right) \\ -\frac{\omega_s}{\eta c} \sin\left(\frac{\omega_s s}{c}\right) & \cos\left(\frac{\omega_s s}{c}\right) \end{pmatrix} \begin{pmatrix} z_0 \\ \delta_0 \end{pmatrix} \quad (6)$$

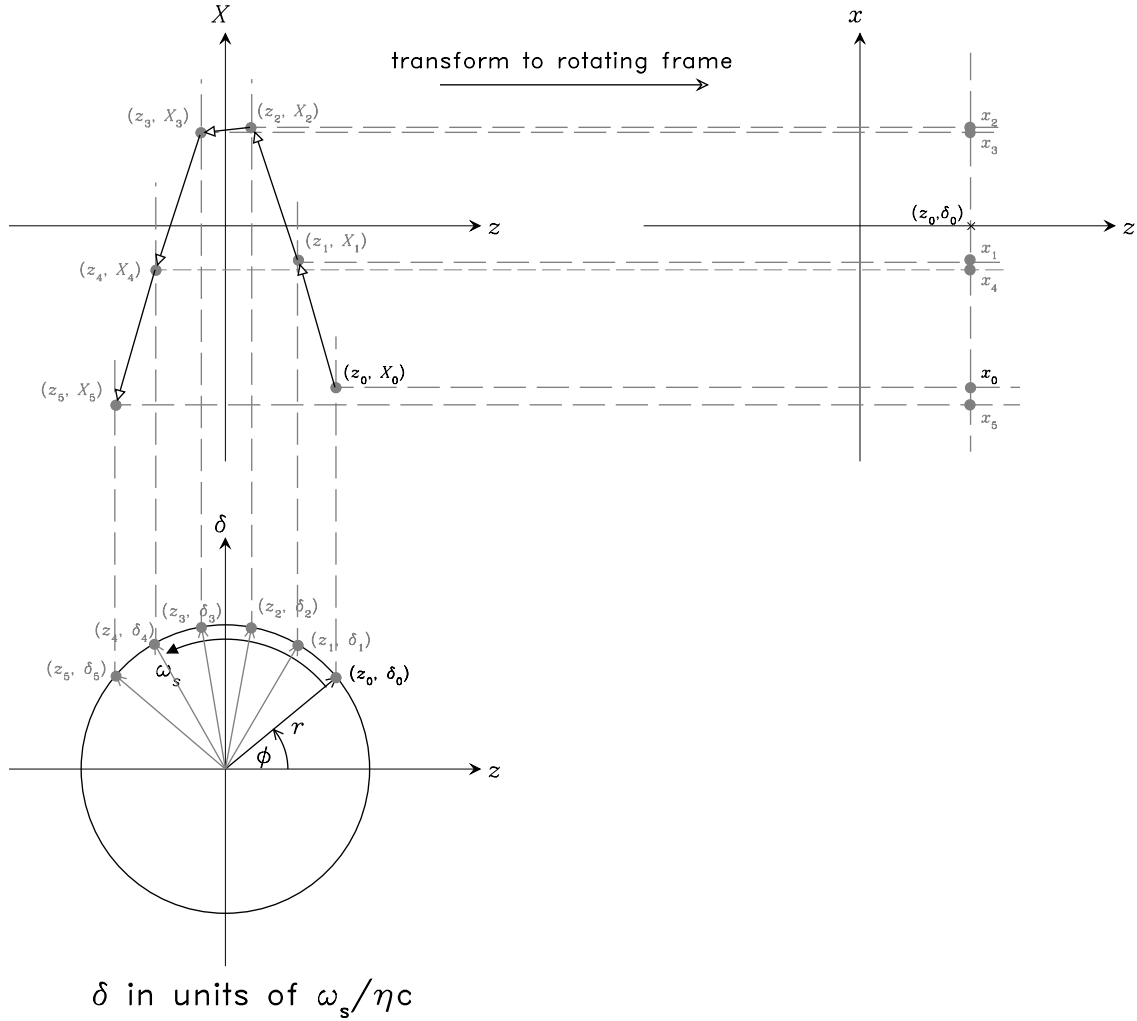


Figure 2 The δ -axis is in units of $-\omega_s/\eta c$ so that the particle at (z_0, δ_0) rotates along a circle at frequency ω_s . In the (z, X) plane, the particle moves along a path that satisfies the o.d.e. (4). After transforming to a rotating frame, the particle oscillates along the line z_0 and satisfies the o.d.e. (7). The 3-D representation is drawn in Figure 8.

We can also think of the map given by (6) as a frame that is rotating at the synchrotron

frequency. Thus in this frame, (4) becomes

$$\frac{d^2x(s, \delta, z)}{ds^2} + \omega_0^2 \left[Q + \xi \left(\delta_0 \cos\left(\frac{\omega_s s}{c}\right) - \frac{\omega_s \tau_0}{\eta} \sin\left(\frac{\omega_s s}{c}\right) \right) \right]^2 x(s, \delta, z) = 0 \quad (7)$$

where $\tau_0 = z_0/c$ and we have mapped $X \rightarrow x$ to remind us that we are in the rotating frame. Next, let us change variables to use turns n rather than s , i.e.

$$n = \frac{s}{2\pi R} \quad \Rightarrow \quad \frac{dn}{ds} = \frac{1}{2\pi R} \quad (8)$$

where R is the radius of the accelerator. In this variable, (7) becomes

$$\frac{d^2x}{dn^2} + \left[2\pi Q + 2\pi\xi \left(\delta_0 \cos(2\pi Q_s n) - \frac{\omega_s \tau_0}{\eta} \sin(2\pi Q_s n) \right) \right]^2 x = 0 \quad (9)$$

where $s/c = 2\pi n/\omega_0$, $Q_s = \omega_s/\omega_0$ is the synchrotron tune.

If the weak sinusoidal kick from the tune tracker PLL is given by $\epsilon\lambda \cos(2\pi Q_k n)$ where $\epsilon \ll 1$, Q_k is the frequency of the kick in tune units and $\lambda = 1$ has the same dimensions as x to keep the dimensions of the lhs and rhs of the o.d.e. correct, then (9) with this force is

$$\ddot{x} + \left[2\pi Q + 2\pi\xi \left(\delta_0 \cos(2\pi Q_s n) - \frac{\omega_s \tau_0}{\eta} \sin(2\pi Q_s n) \right) \right]^2 x = \epsilon\lambda \cos 2\pi Q_k n \quad (10)$$

where $\frac{d}{dn} = \text{“”}$.

Let us define the following new variables so that it is easier to lug (10) around

$$\left. \begin{array}{l} \theta_Q \equiv 2\pi Q \quad \theta_s \equiv 2\pi Q_s \quad \theta_k \equiv 2\pi Q_k \\ \nu \equiv 2\pi\xi\delta_0 \ll 1 \quad \mu \equiv -2\pi\xi\omega_s\tau_0/\eta \ll 1 \end{array} \right\} \quad (11)$$

Thus (10) becomes

$$\left. \begin{array}{l} \ddot{x} + (\theta_Q + \nu \cos n\theta_s + \mu \sin n\theta_s)^2 x = \ddot{x} + \left(\theta_Q^2 + 2\theta_Q\nu \cos n\theta_s + 2\theta_Q\mu \sin n\theta_s + \right. \\ \quad \left. 2\nu\mu \sin n\theta_s \cos n\theta_s + \nu^2 \cos^2 n\theta_s + \mu^2 \sin^2 n\theta_s + \right) x \\ \equiv \ddot{x} + W(n)^2 x = \epsilon\lambda \cos n\theta_k \end{array} \right\} \quad (12)$$

It is clear that (12) is Hill's equation with an external periodic forcing because $W(n) = W(n + 2\pi/\theta_s)$. Directly solving (12) to obtain analytic answers is beyond our capabilities.

Instead, we will solve (12) approximately by using the Averaging Method. However, we have to be careful with the averaging method because according to Arnold⁵, the principle behind the averaging method “is neither a theorem, an axiom nor a definition, but rather a physical proposition, i.e., a vaguely formulated and, strictly speaking, untrue assertion. Such assertions are often fruitful sources of mathematical theorems.” Thus to check that our approximate solutions are close to the real ones, we first assume that the solution obtained by numerically integrating (12) does indeed give us the actual solutions. We will then show that the approximations obtained from the averaging method are really close to the numerical solutions.

Single Particle Solution

To solve (12), we transfer $W(n)^2x$ to the rhs

$$\left. \begin{aligned} \ddot{x} &= \epsilon\lambda \cos n\theta_k - W(n)^2x \\ &\equiv \epsilon g(n; \theta) + f(n, x; \theta_Q, \theta_s, \nu, \mu), \quad x(0) = x_0, \dot{x}(0) = \dot{x}_0 \end{aligned} \right\} \quad (13)$$

Let us write (13) as a system of two first order differential equations:

$$\left. \begin{aligned} \dot{x} &= u \\ \dot{u} &= \epsilon g(n; \theta_k) + f(n, x; \theta_Q, \theta_s, \nu, \mu) \end{aligned} \right\} \quad (14)$$

with $x(0) = x_0$ and $\dot{x}(0) = \dot{x}_0 \equiv u_0 = u(0)$. These equations can be written as one vector equation

$$\dot{\mathbf{x}} = \epsilon \mathbf{g}(n; \theta_k) + \mathbf{f}(n, \mathbf{x}; \theta_Q, \theta_s, \nu, \mu), \quad \mathbf{x}(0) = \mathbf{x}_0 \quad (15)$$

where \mathbf{x} , \mathbf{f} and \mathbf{g} are vectors in \mathbb{R}^2 with the entries of each of these vectors coming from (14). We want to reformulate (15) into the standard form for averaging. See Sanders⁶ or (67) in *Appendix I*. In order to do so, let us consider the unperturbed problem, i.e. when $\epsilon = 0$,

$$\dot{\mathbf{y}} = \mathbf{f}(n, \mathbf{y}; \theta_Q, \theta_s, \nu, \mu), \quad \mathbf{y}(0) = \mathbf{x}_0 \quad (16)$$

In general, (16) cannot be solved in terms of elementary functions. However, if we assume that we can either do it exactly or approximately, then we can apply the *Method of Variation of Parameters* which tells us to treat the constants calculated from initial conditions as functions of n , i.e. if the notation for the homogeneous solution which includes the initial conditions is $\mathbf{y}(n, \mathbf{x}_0)$ then

$$\mathbf{y} = \mathbf{y}(n, \mathbf{z}), \quad \mathbf{y}(0, \mathbf{z}) = \mathbf{z}, \quad \mathbf{z} \in \mathbb{R}^2 \quad (17)$$

where \mathbf{z} is a function of n . To solve the o.d.e. (15) for \mathbf{x} given \mathbf{y} , the method of variation of parameters tells us to let

$$\mathbf{x} = \mathbf{y}(n, \mathbf{z}) \quad (18)$$

and then substitute it into (15), to get

$$\dot{\mathbf{y}} = \frac{\partial \mathbf{y}}{\partial n} + \frac{\partial \mathbf{y}}{\partial \mathbf{z}} \dot{\mathbf{z}} = \epsilon \mathbf{g}(n; \theta_k) + \mathbf{f}(n, \mathbf{y}; \theta_Q, \theta_s, \nu, \mu), \quad (19)$$

But $\partial \mathbf{y} / \partial n$ is the solution of the unperturbed problem, and so (19) becomes

$$\dot{\mathbf{z}} = \epsilon \left[\frac{\partial \mathbf{y}(n, \mathbf{z})}{\partial \mathbf{z}} \right]^{-1} \mathbf{g}(n; \theta) \quad (20)$$

if $\left[\frac{\partial \mathbf{y}(n, \mathbf{z})}{\partial \mathbf{z}} \right]^{-1}$ is nonsingular.

If (20) can be solved for \mathbf{z} , then we have the solution for \mathbf{x} because $\mathbf{x} = \mathbf{y}(n, \mathbf{z})$. However, (20) is usually not easily solved, but fortunately it is in the standard form for applying the averaging method which allows us to find an approximate \mathbf{z} solution. Thus we start our solution of (13) by calculating the homogeneous solution in the next section.

Homogeneous Solution

The original o.d.e. (12) with the rhs set to zero is

$$\ddot{y}_h + W(n)^2 y_h = 0 \quad (21)$$

where we have introduced y_h to be the solution to this equation. A crude solution that is surprisingly accurate is

$$y_h = \phi_0 e^{\pm i \int W(n) dn} \quad (22)$$

where $\phi_0 \in \mathbb{C}$ is a constant determined from initial conditions. Let us just look at the phase term

$$\left. \begin{aligned} \int W(n) dn &= \int \left(\theta_Q + \nu \cos n\theta_s + \mu \sin n\theta_s \right) dn \\ &= n\theta_Q + \frac{1}{\theta_s} \left(\nu \sin n\theta_s - \mu \cos n\theta_s \right) \\ &= n\theta_Q + \frac{\rho}{\theta_s} \sin(n\theta_s - \varphi) \end{aligned} \right\} \quad (23)$$

where

$$\left. \begin{aligned} \rho &= \sqrt{\nu^2 + \mu^2} \\ \varphi &= \tan^{-1} \frac{\mu}{\nu} \end{aligned} \right\} \quad (24)$$

Therefore, the homogeneous solution is

$$\left. \begin{aligned} y_h &= \phi_{01} \cos \left[n\theta_Q + \frac{\rho}{\theta_s} \sin(n\theta_s - \varphi) \right] + \phi_{02} \sin \left[n\theta_Q + \frac{\rho}{\theta_s} \sin(n\theta_s - \varphi) \right] \\ &\equiv \phi_{01} y_1(n) + \phi_{02} y_2(n) \end{aligned} \right\} \quad (25)$$

where $\phi_{01}, \phi_{02} \in \mathbb{R}$ are constants derived from initial conditions.

Variation of Parameters

Let us continue with the prescription for deriving the differential equations which satisfy the Averaging Theorem. The method of variation of parameters is the next step.

The two relevant equations for this method are

$$\left. \begin{aligned} y_h &= \phi_{01} y_1 + \phi_{02} y_2 \\ \dot{y}_h &= \phi_{01} \dot{y}_1 + \phi_{02} \dot{y}_2 \end{aligned} \right\} \quad (26)$$

When we replace ϕ_{01} by $z_1(n)$ and ϕ_{02} by $z_2(n)$, we get

$$\left. \begin{aligned} y &= z_1(n) y_1(n) + z_2(n) y_2(n) \\ \dot{y} &= z_1(n) \dot{y}_1(n) + z_2(n) \dot{y}_2(n) \end{aligned} \right\} \quad (27)$$

We can write down the matrix $\frac{\partial \mathbf{y}}{\partial \mathbf{z}}$ immediately by reading off the coefficients of z_1 and z_2 from (27)

$$\frac{\partial \mathbf{y}}{\partial \mathbf{z}} = \begin{pmatrix} y_1 & y_2 \\ \dot{y}_1 & \dot{y}_2 \end{pmatrix} \quad (28)$$

The matrix equation which relates $\dot{\mathbf{z}}$ to \mathbf{g} comes from (20)

$$\begin{pmatrix} \dot{z}_1 \\ \dot{z}_2 \end{pmatrix} = \epsilon \begin{pmatrix} y_1 & y_2 \\ \dot{y}_1 & \dot{y}_2 \end{pmatrix}^{-1} \begin{pmatrix} 0 \\ g \end{pmatrix} \quad (29)$$

which is exactly the form required for averaging. Multiplying out (29) we get

$$\left. \begin{aligned} \dot{z}_1 &= -\frac{\epsilon y_2 g}{y_1 \dot{y}_2 - \dot{y}_1 y_2} \\ \dot{z}_2 &= \frac{\epsilon y_1 g}{y_1 \dot{y}_2 - \dot{y}_1 y_2} \end{aligned} \right\} \quad (30)$$

The expression $y_1 \dot{y}_2 - \dot{y}_1 y_2$ is called the Wronskian \mathcal{W} . Substituting in y_1 and y_2 from (25) and doing the respective differentials, we find that

$$\left. \begin{aligned} \mathcal{W} &= y_1 \dot{y}_2 - \dot{y}_1 y_2 \\ &= \rho \cos(n\theta_s - \varphi) + \theta_Q \end{aligned} \right\} \quad (31)$$

Therefore, (30) with the rhs expanded is

$$\left. \begin{aligned} \dot{z}_1 &= -\frac{\epsilon \lambda \cos n\theta_k}{\theta_Q} \times \frac{\sin \left[n\theta_Q + \frac{\rho}{\theta_s} \sin(n\theta_s - \varphi) \right]}{\left[1 + \frac{\rho}{\theta_Q} \cos(n\theta_s - \varphi) \right]} \\ &\approx -\frac{\epsilon \lambda \cos n\theta_k}{\theta_Q} \times \sin \left[n\theta_Q + \frac{\rho}{\theta_s} \sin(n\theta_s - \varphi) \right] \times \left[1 - \frac{\rho}{\theta_Q} \cos(n\theta_s - \varphi) \right] \\ \dot{z}_2 &= +\frac{\epsilon \lambda \cos n\theta_k}{\theta_Q} \times \frac{\cos \left[n\theta_Q + \frac{\rho}{\theta_s} \cos(n\theta_s - \varphi) \right]}{\left[1 + \frac{\rho}{\theta_Q} \cos(n\theta_s - \varphi) \right]} \\ &\approx +\frac{\epsilon \lambda \cos n\theta_k}{\theta_Q} \times \cos \left[n\theta_Q + \frac{\rho}{\theta_s} \sin(n\theta_s - \varphi) \right] \times \left[1 - \frac{\rho}{\theta_Q} \cos(n\theta_s - \varphi) \right] \end{aligned} \right\} \quad (32)$$

if we assume that $\rho/\theta_Q \ll 1$.

Averaging

Notice that the rhs of (32) is not periodic but almost periodic because of the three tunes θ_k , θ_Q and θ_s . Therefore, we cannot use the usual Averaging Theorems but have to use

the *Nonlinear Averaging Theorems* described in *Appendix I*. The definition of averaging of a function $f(t_1, t_2, \dots)$ w.r.t. t_1 in this theorem is

$$\bar{f}(t_2, t_3, \dots) \equiv \lim_{T \rightarrow \infty} \frac{1}{T} \int_0^T \sum_{n=0}^{\infty} f_n(t_1, t_2, \dots) e^{i\omega_n t_1} dt_1 \quad (33)$$

Therefore, in this context, $n\theta_Q$ and $n\theta_s$ are treated as independent variables when we perform averaging.

Furthermore, we will find solutions for only two cases because the tune tracker PLL is always assumed to lock onto the betatron tune $\theta_k = \theta_Q$ or close to it i.e. $|\theta_k - \theta_Q| \ll 1$.

Case I: $\theta_k = \theta_Q$

For the case, when the tune tracker PLL is exactly on the betatron tune, $\theta_k = \theta_Q$, when we average the rhs of (32) over $n\theta_Q$, we get

$$\left. \begin{aligned} \dot{\bar{z}}_1 &= -\frac{\epsilon\lambda}{2\theta_Q} \sin \left[\frac{\rho}{\theta_s} \sin(n\theta_s - \varphi) \right] \times \left[1 - \frac{\rho}{\theta_Q} \cos(n\theta_s - \varphi) \right] \\ \dot{\bar{z}}_2 &= \frac{\epsilon\lambda}{2\theta_Q} \cos \left[\frac{\rho}{\theta_s} \sin(n\theta_s - \varphi) \right] \times \left[1 - \frac{\rho}{\theta_Q} \cos(n\theta_s - \varphi) \right] \end{aligned} \right\} \quad (34)$$

which we still cannot easily integrate. Let's go one step further and assume that $\rho/\theta_s \ll 1$, so that the rhs of both $\dot{\bar{z}}_1$ and $\dot{\bar{z}}_2$ become linearised

$$\left. \begin{aligned} \dot{\bar{z}}_1 &= -\frac{\epsilon\lambda}{2\theta_Q} \times \left[\frac{\rho}{\theta_s} \sin(n\theta_s - \varphi) \right] \times \left[1 - \frac{\rho}{\theta_Q} \cos(n\theta_s - \varphi) \right] \\ &\approx -\frac{\epsilon\lambda\rho}{2\theta_Q\theta_s} \sin(n\theta_s - \varphi) \\ \dot{\bar{z}}_2 &= \frac{\epsilon\lambda}{2\theta_Q} \times \left[1 - \frac{\rho}{\theta_Q} \cos(n\theta_s - \varphi) \right] \\ &\approx \frac{\epsilon\lambda}{2\theta_Q} \end{aligned} \right\} \quad (35)$$

where we have used $(\rho/\theta_Q)^2 \approx 0$ and $\rho/\theta_Q^2 \approx 0$. Finally, we can integrate (35) to get

$$\left. \begin{aligned} \bar{z}_1 &= \frac{\epsilon\lambda\rho}{2\theta_Q\theta_s^2} \cos(n\theta_s - \varphi) \\ \bar{z}_2 &= \frac{\epsilon\lambda}{2\theta_Q} n \end{aligned} \right\} \quad (36)$$

Therefore, the particular integral from (27) is

$$\begin{aligned}
 y_p &= \bar{z}_1 y_1 + \bar{z}_2 y_2 \\
 &= \frac{\epsilon \lambda \rho}{2\theta_Q \theta_s^2} \cos(n\theta_s - \varphi) \times \cos \left[n\theta_Q + \frac{\rho}{\theta_s} \sin(n\theta_s - \varphi) \right] + \\
 &\quad \frac{\epsilon \lambda}{2\theta_Q} n \sin \left[n\theta_Q + \frac{\rho}{\theta_s} \sin(n\theta_s - \varphi) \right]
 \end{aligned}
 \tag{37}$$

For large n , the the secular term (i.e. the term which grows with n) dominates and so

$$y = \frac{\epsilon \lambda}{2\theta_Q} n \sin \left[n\theta_Q + \frac{\rho}{\theta_s} \sin(n\theta_s - \varphi) \right]
 \tag{38}$$

In summary, the complete solution to (12) when $\theta_k = \theta_Q$ is

$$\begin{aligned}
 y &= y_h + y_p \\
 &= \left[\phi_{01} + \frac{\epsilon \lambda \rho}{2\theta_Q \theta_s^2} \cos(n\theta_s - \varphi) \right] \times \cos \left[n\theta_Q + \frac{\rho}{\theta_s} \sin(n\theta_s - \varphi) \right] + \\
 &\quad \left[\phi_{02} + \frac{\epsilon \lambda}{2\theta_Q} n \right] \times \sin \left[n\theta_Q + \frac{\rho}{\theta_s} \sin(n\theta_s - \varphi) \right]
 \end{aligned}
 \tag{39}$$

Numerical Check

We will compare the solution obtained by the averaging method to the numerically integrated solution of the o.d.e. (10). The FORTRAN o.d.e. solver which we have used is written by R.W. Brankin *et al* and it is based on Runge-Kutta formulæ.⁷ The numerical parameters used for comparing the two methods are shown in Table 1.

Table 1. Parameters used in the simulation

Parameter	Value	Parameter	Value
Q	20.575	Q_s	1.77×10^{-3}
ξ	3	δ_0	10^{-4}
$\omega_s \tau_0$	7.959×10^{-7}	η	0.0028
ϵ	0.01	-	-
$y(0)$	0.01	$\dot{y}(0)$	0

The two solutions when plotted on top of each other and the relative error between the two solutions are shown in Figure 3. The zoomed in view shows that these two solutions are very close. The calculation of the relative errors between the two solutions require cuts because points close to zero crossings produce large relative errors but the absolute errors remain small. Any points between $y = \pm 0.25 \times 10^{-2}$ are not used to calculate the relative error but immediately set to zero. From here we can see that the averaging method produces a solution that is about 5% larger than the Runge-Kutta solution. Even with the cuts, there are sharp spikes that show that there are relative errors of about 25%.

Case II: $|\theta_k - \theta_Q| \ll 1$

Suppose the tune tracker PLL locks close to but not right on θ_Q , i.e. $|\theta_k - \theta_Q| \ll 1$.

Let us write

$$\theta_k = \theta_Q + \delta\theta_Q \tag{40}$$

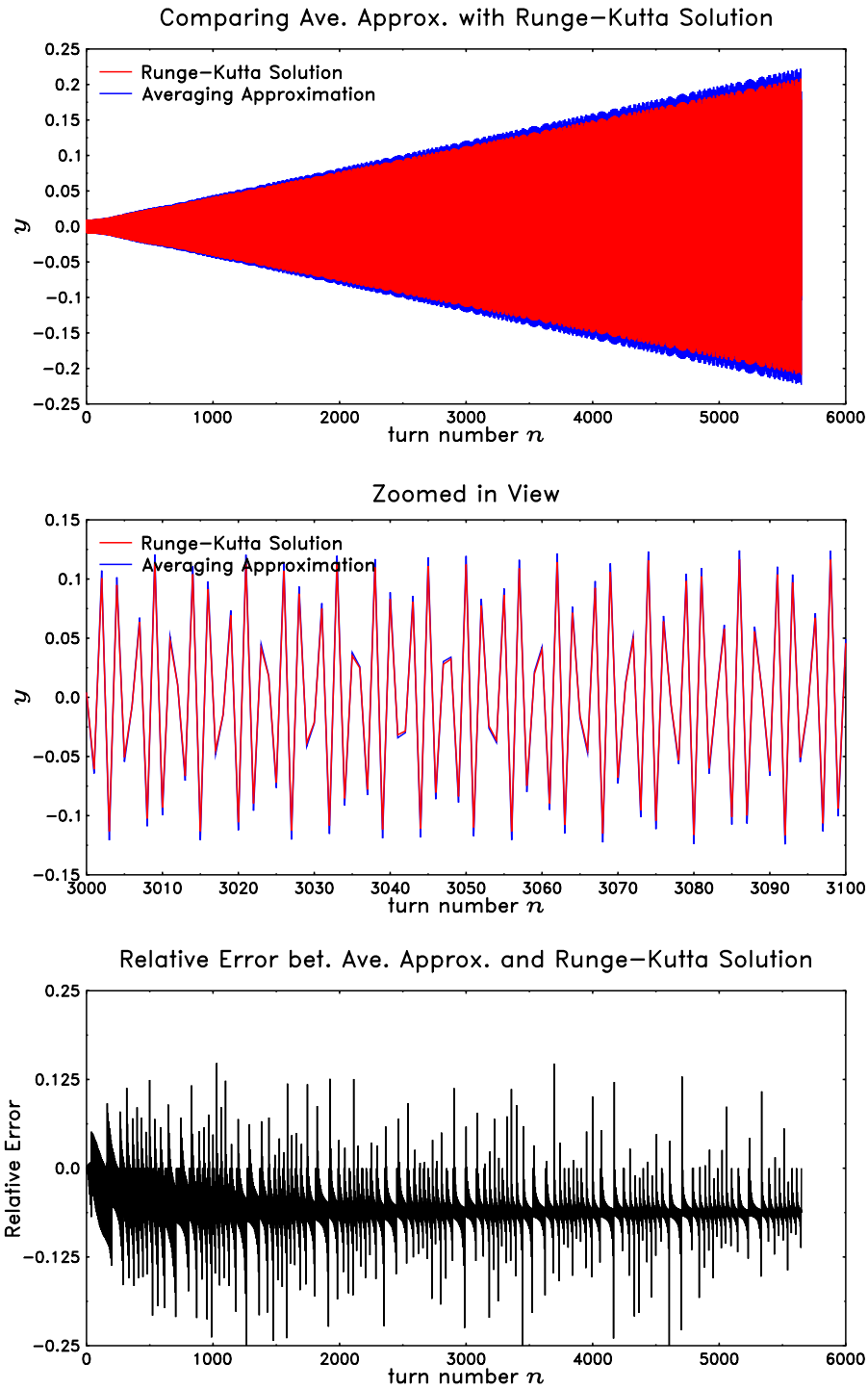


Figure 3 This compares the two solutions obtained by using the averaging method and the Runge-Kutta solver. The relative error between the two solutions is $< 25\%$. See text.

When we substitute this into (32) we get

$$\left. \begin{aligned} \dot{z}_1 &= -\frac{\epsilon\lambda}{\theta_Q} \left(\cos n\theta_Q \cos n\delta\theta_Q - \sin n\theta_Q \sin n\delta\theta_Q \right) \times \\ &\quad \left(\sin n\theta_Q \cos \left[\frac{\rho}{\theta_s} \sin(n\theta_s - \varphi) \right] + \cos n\theta_Q \sin \left[\frac{\rho}{\theta_s} \sin(n\theta_s - \varphi) \right] \right) \\ \dot{z}_2 &= +\frac{\epsilon\lambda}{\theta_Q} \left(\cos n\theta_Q \cos n\delta\theta_Q - \sin n\theta_Q \sin n\delta\theta_Q \right) \times \\ &\quad \left(\cos n\theta_Q \cos \left[\frac{\rho}{\theta_s} \sin(n\theta_s - \varphi) \right] - \sin n\theta_Q \sin \left[\frac{\rho}{\theta_s} \sin(n\theta_s - \varphi) \right] \right) \end{aligned} \right\} \quad (41)$$

if $\rho/\theta_Q^2 \approx 0$. When we average over $n\theta_Q$ as before, we get

$$\left. \begin{aligned} \dot{\bar{z}}_1 &= \frac{\epsilon\lambda}{2\theta_Q} \left[\sin n\delta\theta_Q - \frac{\rho}{\theta_s} \cos n\delta\theta_Q \sin(n\theta_s - \varphi) \right] \\ \dot{\bar{z}}_2 &= \frac{\epsilon\lambda}{2\theta_Q} \left[\cos n\delta\theta_Q + \frac{\rho}{\theta_s} \sin n\delta\theta_Q \sin(n\theta_s - \varphi) \right] \end{aligned} \right\} \quad (42)$$

if we assume that $\rho/\theta_s \ll 1$. (42) is actually integrable and so we get

$$\left. \begin{aligned} \bar{z}_1 &= -\frac{\epsilon\lambda}{2\theta_Q} \left(\frac{\cos n\delta\theta_Q}{\delta\theta_Q} - \right. \\ &\quad \left. \frac{\rho}{\theta_s(\delta\theta_Q^2 - \theta_s^2)} \left[\theta_s \cos n\delta\theta_Q \cos(n\theta_s - \varphi) + \delta\theta_Q \sin n\delta\theta_Q \sin(n\theta_s - \varphi) \right] \right) \\ \bar{z}_2 &= +\frac{\epsilon\lambda}{2\theta_Q} \left(\frac{\sin n\delta\theta_Q}{\delta\theta_Q} - \right. \\ &\quad \left. \frac{\rho}{\theta_s(\delta\theta_Q^2 - \theta_s^2)} \left[\theta_s \sin n\delta\theta_Q \cos(n\theta_s - \varphi) - \delta\theta_Q \cos n\delta\theta_Q \sin(n\theta_s - \varphi) \right] \right) \end{aligned} \right\} \quad (43)$$

As expected, as $\delta\theta_Q \rightarrow 0$, $\cos n\delta\theta_Q/\delta\theta_Q \rightarrow \infty$ in the \bar{z}_1 equation. This singularity will be removed when the initial conditions are included in the full solution. See Chao⁸. The secular term arises when $\delta\theta_Q \rightarrow 0$, $\sin n\delta\theta_Q/\delta\theta_Q \rightarrow n$, which is exactly the secular term of (37). Furthermore, we notice that there are extra singularities which occur when $\delta\theta_Q = \pm\theta_s$.

Carrying on, we can calculate the particular integral from (27)

$$\begin{aligned}
y_p &= \bar{z}_1 y_1 + \bar{z}_2 y_2 \\
&= \frac{\epsilon \lambda}{2\theta_Q} \left\{ -\frac{\cos n\delta\theta_Q}{\delta\theta_Q} \cos \left[n\theta_Q + \frac{\rho}{\theta_s} \sin(n\theta_s - \varphi) \right] + \right. \\
&\quad \left. \frac{\sin n\delta\theta_Q}{\delta\theta_Q} \sin \left[n\theta_Q + \frac{\rho}{\theta_s} \sin(n\theta_s - \varphi) \right] + \right. \\
&\quad \left. \frac{\rho}{2\theta_s} \left(\frac{1}{\delta\theta_Q + \theta_s} \cos \left[n(\theta_Q + \delta\theta_Q) + \frac{\rho}{\theta_s} \sin(n\theta_s - \varphi) + (n\theta_s - \varphi) \right] - \right. \right. \\
&\quad \left. \left. \frac{1}{\delta\theta_Q - \theta_s} \cos \left[n(\theta_Q + \delta\theta_Q) + \frac{\rho}{\theta_s} \sin(n\theta_s - \varphi) - (n\theta_s - \varphi) \right] \right) \right\} \quad (44)
\end{aligned}$$

which when we take $\delta\theta_Q \rightarrow 0$, we see that the result is the same as (37) except for the singularity when $\cos n\delta\theta_Q/\delta\theta_Q$ when $\delta\theta_Q \rightarrow 0$.

Therefore, the complete solution to (10) when $\theta_k - \theta_Q = \delta\theta_Q$ is

$$\begin{aligned}
y &= y_h + y_p \\
&= \left(\phi_{01} - \frac{\epsilon \lambda \cos n\delta\theta_Q}{2\theta_Q \delta\theta_Q} \right) \cos \left[n\theta_Q + \frac{\rho}{\theta_s} \sin(n\theta_s - \varphi) \right] + \\
&\quad \left(\phi_{02} + \frac{\epsilon \lambda \sin n\delta\theta_Q}{2\theta_Q \delta\theta_Q} \right) \sin \left[n\theta_Q + \frac{\rho}{\theta_s} \sin(n\theta_s - \varphi) \right] + \\
&\quad \frac{\epsilon \lambda \rho}{4\theta_Q \theta_s} \left(\frac{1}{\delta\theta_Q + \theta_s} \cos \left[n(\theta_Q + \delta\theta_Q) + \frac{\rho}{\theta_s} \sin(n\theta_s - \varphi) + (n\theta_s - \varphi) \right] - \right. \\
&\quad \left. \frac{1}{\delta\theta_Q - \theta_s} \cos \left[n(\theta_Q + \delta\theta_Q) + \frac{\rho}{\theta_s} \sin(n\theta_s - \varphi) - (n\theta_s - \varphi) \right] \right) \quad (45)
\end{aligned}$$

If we put in the initial conditions $y(0) = 0$ and $\dot{y}(0) = 0$, we see that

$$\begin{aligned}
y &= \frac{\epsilon \lambda}{2\theta_Q \delta\theta_Q} (1 - \cos n\delta\theta_Q) \cos \left[n\theta_Q + \frac{\rho}{\theta_s} \sin(n\theta_s - \varphi) \right] + \\
&\quad \frac{\epsilon \lambda}{2\theta_Q \delta\theta_Q} \sin n\delta\theta_Q \sin \left[n\theta_Q + \frac{\rho}{\theta_s} \sin(n\theta_s - \varphi) \right] + \dots \quad (46)
\end{aligned}$$

And as we have promised earlier, the initial conditions have taken care of the singularity at $\cos n\delta\theta_Q/\delta\theta_Q$, because as $\delta\theta_Q \rightarrow 0$, $(1 - \cos n\delta\theta_Q)/\delta\theta_Q \rightarrow 0$ and is therefore well behaved.

(Note: other initial conditions will also take care of this singularity.)

Numerical Check

Like before, we will compare the analytic solutions (45) with the solution which we calculate using the Runge-Kutta method. The parameters of the calculations are for $\omega_s\tau_0 = +7.959 \times 10^{-7}$, $\delta\theta_Q = -0.01$ and those of Table 1. We chose this value of $\delta\theta_Q$ because $|\delta Q| = |\delta\theta_Q|/2\pi \approx 0.0016$ is approximately the minimum accuracy that is required for the tune tracker PLL. With these values, Figure 4 compares the two methods. It is obvious that the two solutions are nearly identical which confirms the validity of the averaging method.

Laboratory Frame

All the calculations that we have done so far are in the frame that follows the single particle. In the laboratory frame, we measure the transverse position of the beam once a turn at the longitudinal positions $\pm\tau_B$ while we continuously kick the beam. To arrive at an analytic solution for this paper, we will make the assumption that the beam is matched to the RF bucket, i.e. in the (τ, δ) plane the particle distribution is stationary⁹. This means that the particles are dense on the contour r_B/c . See Figure 5. The series of pictures here give us a clue for how to calculate the transverse position of the beam at $(r_B/c, \phi_B)$ for all n . Note that the labels $(\hat{\tau}_B, \hat{\delta}_B), (\hat{\tau}_1, \hat{\delta}_2), \dots$, are the initial conditions at $n = 0$ which are used to calculate ϕ_{01} and ϕ_{02} of (39) or (45). Notice that we have used the symbol “^” to denote initial conditions at $n = 0$. At time $n = 0$, the point labeled $(\hat{\tau}_B, \hat{\delta}_B)$ is at the observation point. The point $(\hat{\tau}_1, \hat{\delta}_1)$ is at an angle θ_s away from $(\hat{\tau}_B, \hat{\delta}_B)$. And so at time $n = 1$, $(\hat{\tau}_B, \hat{\delta}_B)$ rotates counter-clockwise away by θ_s and the point $(\hat{\tau}_1, \hat{\delta}_1)$ now lands at the observation point. At $n = 2$, the point $(\hat{\tau}_1, \hat{\delta}_1)$ rotates away by θ_s and the point $(\hat{\tau}_2, \hat{\delta}_2)$ lands at the observation point. This continues *ad infinitum*.

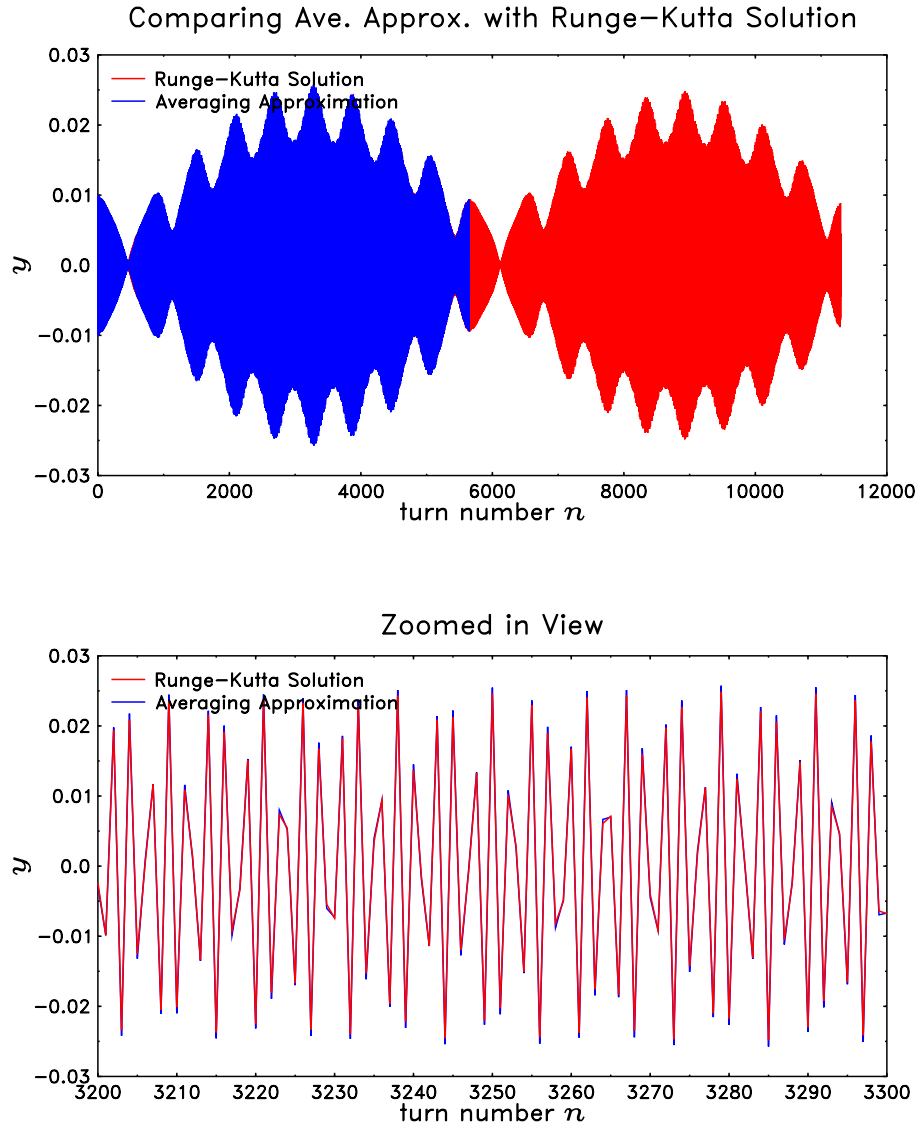


Figure 4 The solution calculated from (45) and Runge-Kutta is shown here. We only show half the number of points for the averaged solution so that the Runge-Kutta solution can be seen. The zoomed in view at an arbitrarily chosen turn shows that the two methods give nearly identical solutions.

Therefore, at the observation point, the transverse amplitude $\hat{Y}_B(n)$ (the symbols are here to remind us that the amplitude is measured at point $(r_B/c, \phi_B)$ and uses initial

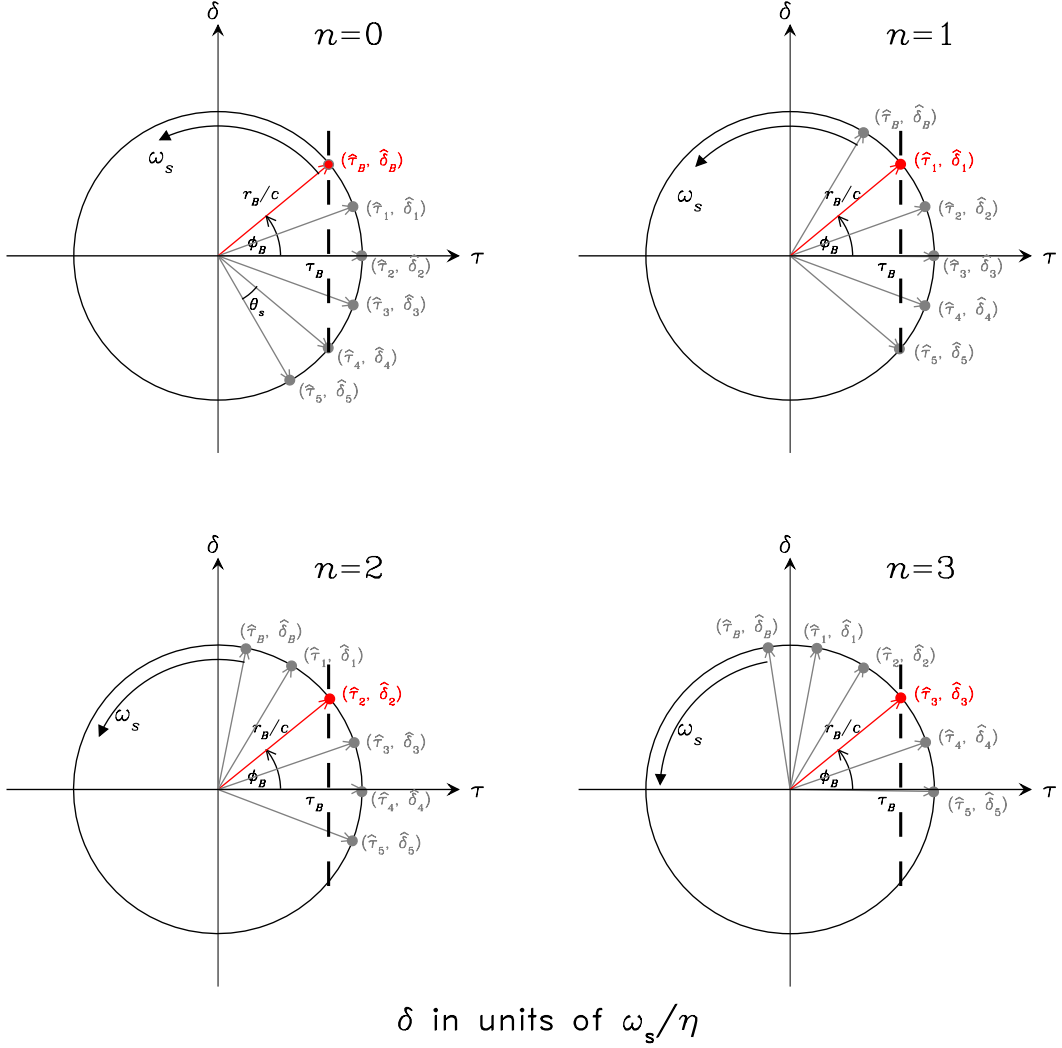


Figure 5 These series of pictures tell us how to calculate the transverse position of the beam at $(r_B/c, \phi_B)$. The angle between each vector is θ_s . Note that the labels $(\hat{\tau}_B, \hat{\delta}_B), (\hat{\tau}_1, \hat{\delta}_1), \dots$, are the initial conditions at $n = 0$ which are used to calculate ϕ_{01} and ϕ_{02} of (39) or (45). Note that the circle r_B/c contains a dense set of points. We only highlight the points which are relevant for the calculation. Note also that $\phi_B - n\theta_s = \hat{\varphi}_B + n\theta_s$ because $\hat{\varphi}_B = \pi/2 - \phi_B$.

and ϕ_{02} in terms of ρ and φ are[†]

$$\left. \begin{aligned} \phi_{01}(\rho, \varphi) &= \epsilon\lambda \left\{ -\frac{1}{4\theta_Q(\theta_Q + \rho \cos \varphi)} \cos\left(\frac{2\rho}{\theta_s} \sin \varphi\right) + \right. \\ &\quad \left. \frac{1}{4\theta_Q\theta_s(\theta_Q + \rho \cos \varphi)} \left[\theta_s - \rho \sin \varphi \sin\left(\frac{2\rho}{\theta_s} \sin \varphi\right) \right] + \frac{1}{2\delta\theta_Q\theta_Q} + \right. \\ &\quad \left. \frac{\rho \cos \varphi}{2(\delta\theta_Q^2 - \theta_s^2)(\theta_Q + \rho \cos \varphi)} \left(1 + \frac{\rho \cos \varphi}{\theta_Q} \right) \right\} \\ \phi_{02}(\rho, \varphi) &= \epsilon\lambda \left\{ \frac{1}{4\theta_Q(\theta_Q + \rho \cos \varphi)} \sin\left(\frac{2\rho}{\theta_s} \sin \varphi\right) - \right. \\ &\quad \left. \frac{\rho \sin \varphi}{2\theta_Q\theta_s} \left(\frac{\cos^2\left(\frac{\rho}{\theta_s} \sin \varphi\right)}{\theta_Q + \rho \cos \varphi} + \frac{\delta\theta_Q}{\delta\theta_Q^2 - \theta_s^2} \right) \right\} \end{aligned} \right\} \quad (50)$$

and so from (49), $\hat{Y}_B(n)$ is easily derived by mapping $\rho \rightarrow \hat{\rho}_B$ and $\varphi \rightarrow (n\theta_s + \hat{\varphi}_B)$ of y .

Thus the analytic solution for the transverse amplitude at $(\hat{\rho}_B, \hat{\varphi}_B)$ for all n is

$$\left. \begin{aligned} \hat{Y}_B(n) &= \left(\phi_{01}(\hat{\rho}_B, n\theta_s + \hat{\varphi}_B) - \frac{\epsilon\lambda \cos n\delta\theta_Q}{2\theta_Q\delta\theta_Q} \right) \cos \left[n\theta_Q - \frac{\hat{\rho}_B}{\theta_s} \sin \hat{\varphi}_B \right] - \\ &\quad \left(\phi_{02}(\hat{\rho}_B, n\theta_s + \hat{\varphi}_B) + \frac{\epsilon\lambda \sin n\delta\theta_Q}{2\theta_Q\delta\theta_Q} \right) \sin \left[n\theta_Q - \frac{\hat{\rho}_B}{\theta_s} \sin \hat{\varphi}_B \right] + \\ &\quad \frac{\epsilon\lambda\hat{\rho}_B}{4\theta_Q\theta_s} \left(\frac{1}{\delta\theta_Q + \theta_s} \cos \left[n(\theta_Q + \delta\theta_Q) - \frac{\hat{\rho}_B}{\theta_s} \sin \hat{\varphi}_B - \hat{\varphi}_B \right] - \right. \\ &\quad \left. \frac{1}{\delta\theta_Q - \theta_s} \cos \left[n(\theta_Q + \delta\theta_Q) - \frac{\hat{\rho}_B}{\theta_s} \sin \hat{\varphi}_B + \hat{\varphi}_B \right] \right) \end{aligned} \right\} \quad (51)$$

It is interesting to note that the time dependent synchrotron term $n\theta_s$ is now embedded in ϕ_{01} and ϕ_{02} and removed from the terms $\cos n\theta_Q$, $\sin n\theta_Q$, $\cos n(\theta_Q + \delta\theta_Q)$ and $\sin n(\theta_Q + \delta\theta_Q)$. The reason why there can be any phase difference between the head and the tail originates from here. This means that if we had ignored the initial conditions, we would have obtained an incorrect solution.

[†] These algebraic solutions have been verified with *Mathematica*.

Numerical Check

We use the same parameters shown in Table 1 to verify (51). We will examine the solution at two different observation points at $(\hat{\tau}_B, \pm\hat{\delta}_B) = (1 \text{ ns}, \pm 10^{-4})$. The comparison between the Runge-Kutta solution and (51) is shown in Figures 6 and 7. Again, the analytic solution is very close to the numeric solution.

Changing Perspective

To calculate the phase difference between the head and tail, we will first change perspective from that of a fixed betatron tune θ_Q and variable kick tune θ_k to that of a fixed θ_k and variable θ_Q because ultimately in our experiment which will be discussed in the section *Experiment* or when we use the tune tracker PLL, we measure phase w.r.t. the frequency of the kick and not the betatron frequency. In this perspective, we have

$$\theta_Q = \theta_k - \delta\theta_Q \quad \text{from (40)} \quad (52)$$

and thus $\hat{Y}_B(n)$ is transformed to this perspective with a trivial change of variables, where we just replace θ_Q with $\theta_k - \delta\theta_Q$ to become

$$\begin{aligned} \hat{Y}_{k,B}(n) = & \left(\phi_{01}(\hat{\rho}_B, n\theta_s + \hat{\varphi}_B) - \frac{\epsilon\lambda \cos n\delta\theta_Q}{2(\theta_k - \delta\theta_Q)\delta\theta_Q} \right) \cos \left[n(\theta_k - \delta\theta_Q) - \frac{\hat{\rho}_B}{\theta_s} \sin \hat{\varphi}_B \right] - \\ & \left(\phi_{02}(\hat{\rho}_B, n\theta_s + \hat{\varphi}_B) + \frac{\epsilon\lambda \sin n\delta\theta_Q}{2(\theta_k - \delta\theta_Q)\delta\theta_Q} \right) \sin \left[n(\theta_k - \delta\theta_Q) - \frac{\hat{\rho}_B}{\theta_s} \sin \hat{\varphi}_B \right] + \\ & \frac{\epsilon\lambda\hat{\rho}_B}{4(\theta_k - \delta\theta_Q)\theta_s} \left(\frac{1}{\delta\theta_Q + \theta_s} \cos \left[n\theta_k - \frac{\hat{\rho}_B}{\theta_s} \sin \hat{\varphi}_B - \hat{\varphi}_B \right] - \right. \\ & \left. \frac{1}{\delta\theta_Q - \theta_s} \cos \left[n\theta_k - \frac{\hat{\rho}_B}{\theta_s} \sin \hat{\varphi}_B + \hat{\varphi}_B \right] \right) \end{aligned} \quad (53)$$

where we have added k to the subscript of $\hat{Y}_{k,B}(n)$ to remind ourselves that we are in the perspective of the kicker and the new functions $\phi_{k,01}()$ and $\phi_{k,02}()$ are $\phi_{01}()$ and $\phi_{02}()$

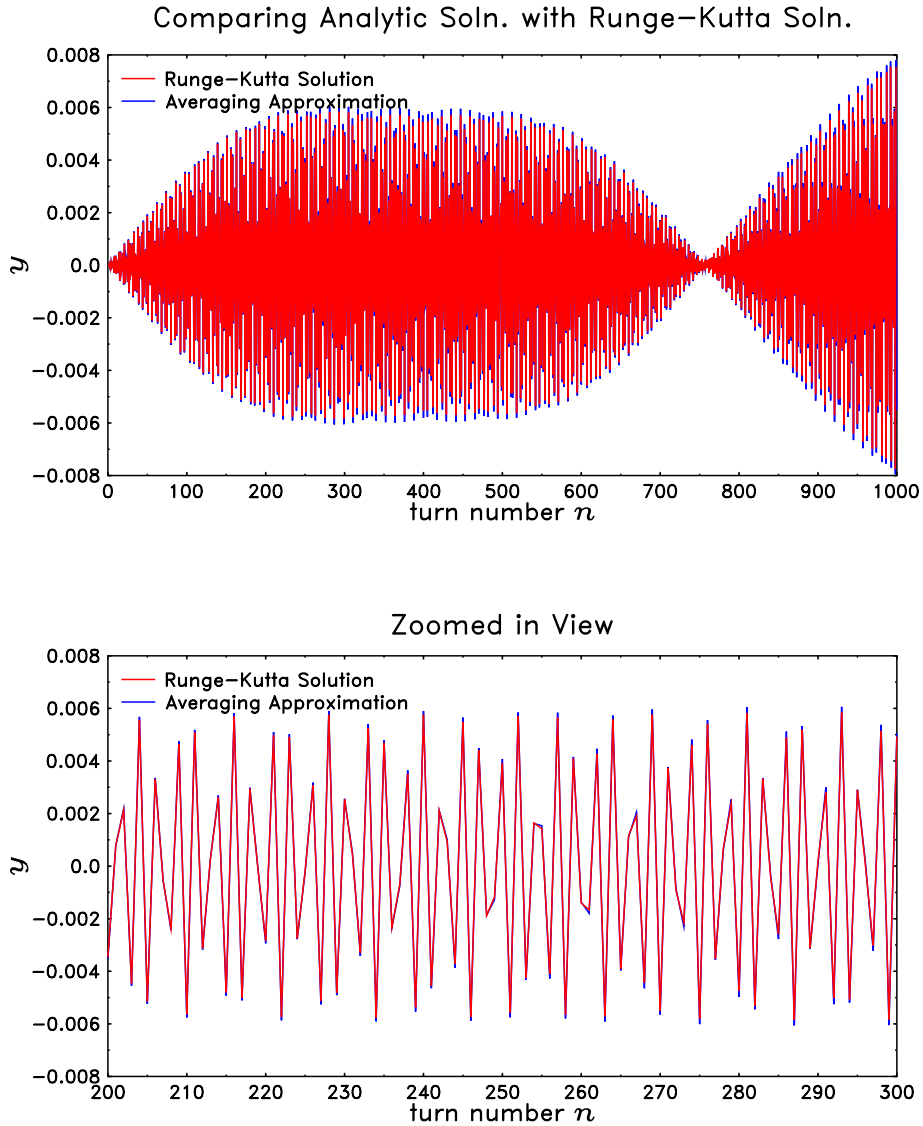


Figure 6 The solution calculated from (51) and Runge-Kutta for the observation point $(\hat{\tau}_B, +\hat{\delta}_B) = (1 \text{ ns}, +10^{-4})$ is shown here. The zoomed in view at an arbitrarily chosen turn shows that the two methods give nearly identical solutions.

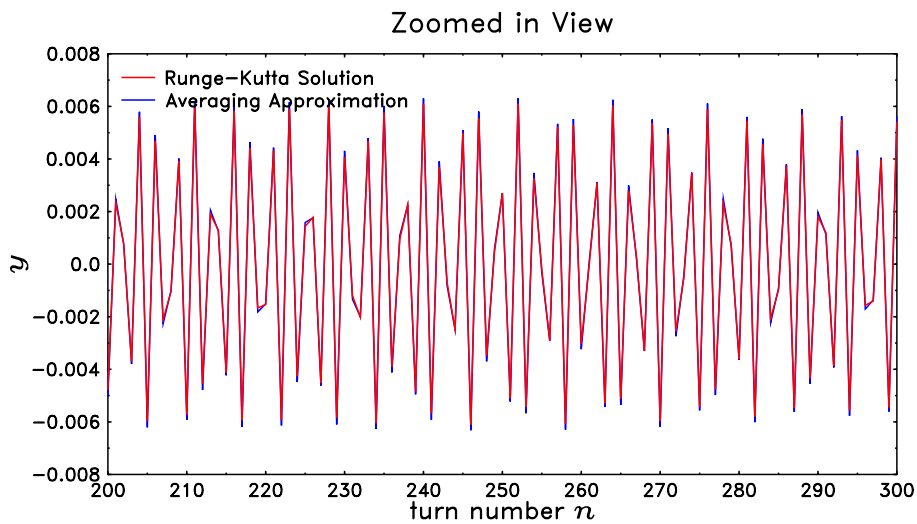
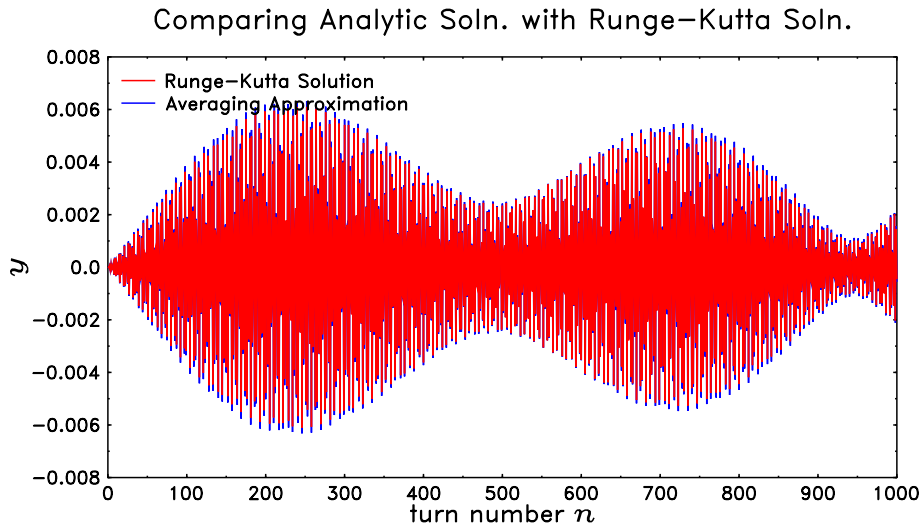


Figure 7 The solution calculated from (51) and Runge-Kutta for the observation point $(\hat{\tau}_B, -\hat{\delta}_B) = (1 \text{ ns}, -10^{-4})$ is shown here. And like Figure 6, the two methods give nearly identical solutions.

with $\theta_Q \rightarrow \theta_k - \delta\theta_Q$ i.e.

$$\begin{aligned}
\phi_{k,01}(\hat{\rho}_B, n\theta_s + \hat{\varphi}_B) &= \epsilon\lambda \left\{ -\frac{\cos\left(\frac{2\hat{\rho}_B}{\theta_s} \sin(n\theta_s + \hat{\varphi}_B)\right)}{4(\theta_k - \delta\theta_Q)(\theta_k - \delta\theta_Q + \hat{\rho}_B \cos(n\theta_s + \hat{\varphi}_B))} + \right. \\
&\quad \left. \frac{\left[\theta_s - \hat{\rho}_B \sin(n\theta_s + \hat{\varphi}_B) \sin\left(\frac{2\hat{\rho}_B}{\theta_s} \sin(n\theta_s + \hat{\varphi}_B)\right)\right]}{4\theta_s(\theta_k - \delta\theta_Q)(\theta_k - \delta\theta_Q + \hat{\rho}_B \cos(n\theta_s + \hat{\varphi}_B))} + \right. \\
&\quad \left. \frac{1}{2(\theta_k - \delta\theta_Q)\delta\theta_Q} + \right. \\
&\quad \left. \frac{\hat{\rho}_B \cos(n\theta_s + \hat{\varphi}_B) \left(1 + \frac{\hat{\rho}_B \cos(n\theta_s + \hat{\varphi}_B)}{\theta_k - \delta\theta_Q}\right)}{2(\delta\theta_Q^2 - \theta_s^2)(\theta_k - \delta\theta_Q + \hat{\rho}_B \cos(n\theta_s + \hat{\varphi}_B))} \right\} \\
\phi_{k,02}(\hat{\rho}_B, n\theta_s + \hat{\varphi}_B) &= \epsilon\lambda \left\{ \frac{\sin\left(\frac{2\hat{\rho}_B}{\theta_s} \sin(n\theta_s + \hat{\varphi}_B)\right)}{4(\theta_k - \delta\theta_Q)(\theta_k - \delta\theta_Q + \hat{\rho}_B \cos(n\theta_s + \hat{\varphi}_B))} - \right. \\
&\quad \left. \frac{\hat{\rho}_B \sin(n\theta_s + \hat{\varphi}_B)}{2(\theta_k - \delta\theta_Q)\theta_s} \left(\frac{\cos^2\left(\frac{\hat{\rho}_B}{\theta_s} \sin(n\theta_s + \hat{\varphi}_B)\right)}{\theta_k - \delta\theta_Q + \hat{\rho}_B \cos(n\theta_s + \hat{\varphi}_B)} + \frac{\delta\theta_Q}{\delta\theta_Q^2 - \theta_s^2} \right) \right\} \\
&\hspace{15em} (54)
\end{aligned}$$

When we look at (53) and (54) — which are rather complicated — very carefully, we can extract out two different cases that are relevant to us. The first is when $|\delta\theta_Q| \ll \theta_s \ll 1$ or $\delta\theta_Q = 0$, i.e. very close to the betatron tune but not on a synchrotron line or on the betatron tune and the second case is when $|\delta\theta_Q| \approx \theta_s \ll 1$ when we are kicking close or on a synchrotron line. The second case is important because for the tune tracker PLL, there is always a possibility that it locks to the closest synchrotron tune w.r.t. the betatron tune and not on the betatron tune itself.

Case A: $|\delta\theta_Q| \ll \theta_s \ll 1$ or $\delta\theta_Q = 0$

In this case, the dominant terms in (53) are those with coefficients which contain $1/\delta\theta_Q$.

Picking these out, we have

$$\hat{Y}_{\delta\theta_Q,k,B}(n) = \frac{\epsilon\lambda}{2(\theta_k - \delta\theta_Q)} \left(\frac{1 - \cos n\delta\theta_Q}{\delta\theta_Q} \cos \left[n(\theta_k - \delta\theta_Q) - \frac{\hat{\rho}_B}{\theta_s} \sin \hat{\varphi}_B \right] - \frac{\sin n\delta\theta_Q}{\delta\theta_Q} \sin \left[n(\theta_k - \delta\theta_Q) - \frac{\hat{\rho}_B}{\theta_s} \sin \hat{\varphi}_B \right] \right) - \left. \begin{aligned} &= -\frac{\epsilon\lambda}{2(\theta_k - \delta\theta_Q)\delta\theta_Q} \left(\cos \left[n(\theta_k - \delta\theta_Q) - n\delta\theta_Q - \frac{\hat{\rho}_B}{\theta_s} \sin \hat{\varphi}_B \right] - \right. \\ &\quad \left. \cos \left[n(\theta_k - \delta\theta_Q) - \frac{\hat{\rho}_B}{\theta_s} \sin \hat{\varphi}_B \right] \right) \end{aligned} \right\} \quad (55)$$

and the string of \hat{Y} subscripts has increased with the addition of $\delta\theta_Q$ which reminds us that we are only looking at terms which contain $1/\delta\theta_Q$.

To obtain an averaged transverse position \hat{X} , we have to integrate \hat{Y} over δ .[†] See Figure 8. Note that the δ distribution is time independent because we have assumed that the (τ, δ) distribution is matched to the bucket and thus stationary. Let $\sigma(\tau_B, \delta) \equiv \sigma(\delta)$ be the density of particles in the (τ, δ) plane which is normalized, i.e.

$$\int_{-\infty}^{\infty} d\delta \sigma(\delta) = 1 \quad (56)$$

Therefore, the fraction of particles in the small segment δ is $\sigma d\delta$ which gives us the weight for calculating the average \hat{X} , i.e.

$$\hat{X}_{\theta_k,k,B} = \int_{-\infty}^{\infty} d\delta \sigma(\delta) \hat{Y}_{\theta_k,k,B} \quad (57)$$

Before we can perform the integral of $\hat{Y}_{\theta_k,k,B}(n)$ over δ , we have to find an expression for $\frac{\rho}{\theta_s} \sin \varphi$ in terms of τ and δ . Figure 9 shows us how to do this

$$\sin \left(\tan^{-1} \theta \right) = \frac{\omega_s |\tau| / \eta}{\sqrt{\left(\frac{\omega_s \tau}{\eta} \right)^2 + \delta^2}} \quad \text{if } \nu, \mu > 0 \quad (58)$$

[†] In general, this integral is 2-dimensional with $\sigma(\tau_B, \delta, X)$, however, because of the initial condition that $y(0) = \dot{y}(0) = 0$, we have a sheet in the (τ, δ, X) space and not a volume.

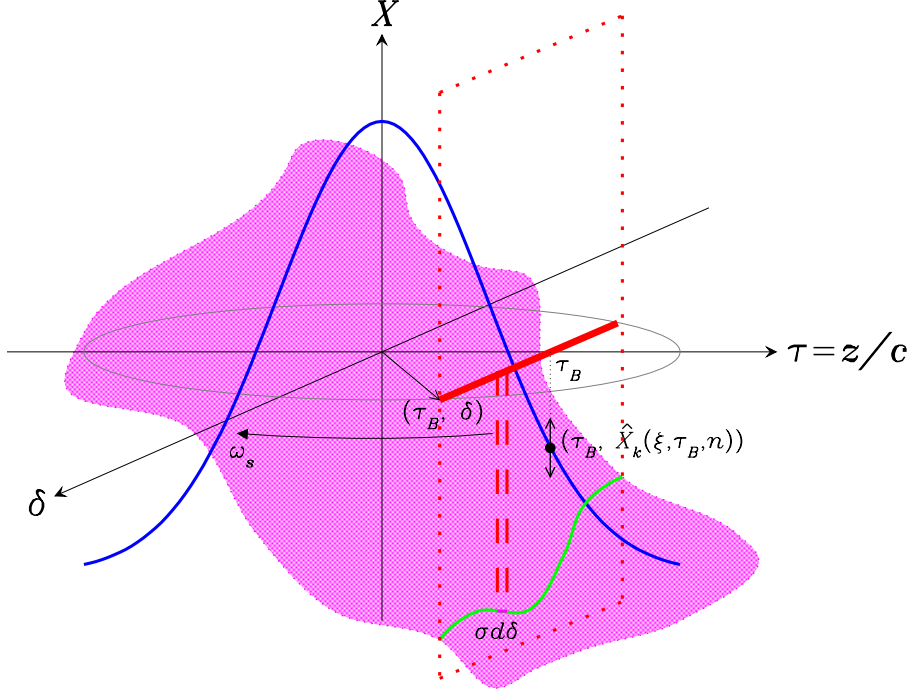
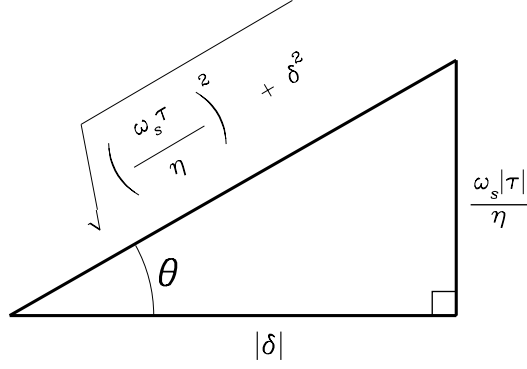


Figure 8 The blue curve represents the bunch signal at a beam position monitor. The point $(\tau_B, \hat{X}_k(\xi, \tau_B, n))$ comes from integrating \hat{Y} over all the particles in the red line and thus gives us an averaged position \hat{X} at τ_B . The magenta surface is the distribution of particles in (τ, δ, X) space. We have a sheet because of the initial conditions. The green line is the intersection between the plane at constant τ_B and the magenta surface.

And so we can produce a cheat sheet for $\frac{\rho}{\theta_s} \sin \varphi$ for different signs of τ and δ from ρ and φ from (24) and μ and ν from (11).

$$\frac{\rho}{\theta_s} \sin \varphi = \begin{cases} -\frac{\xi\omega_0|\tau|}{\eta} & \text{if } \tau > 0 \text{ and } \delta > 0 \\ -\frac{\xi\omega_0|\tau|}{\eta} & \text{if } \tau > 0 \text{ and } \delta < 0 \\ +\frac{\xi\omega_0|\tau|}{\eta} & \text{if } \tau < 0 \text{ and } \delta > 0 \\ +\frac{\xi\omega_0|\tau|}{\eta} & \text{if } \tau < 0 \text{ and } \delta < 0 \end{cases} \quad (59)$$



$$\theta = \tan^{-1}\left(\omega_s |\tau| / \eta |\delta|\right)$$

$$\sin \theta = \sin \tan^{-1}\left(\omega_s |\tau| / \eta |\delta|\right) = \frac{\omega_s |\tau| / \eta}{\sqrt{(\omega_s \tau / \eta)^2 + \delta^2}}$$

Figure 9 This figure shows how we derive (58) for $\nu, \mu > 0$. The sign of $\sin \theta$ must be carefully considered by examining each possible sign of ν and μ .

With this cheat sheet, we can calculate the averaged transverse position \hat{X} at τ_B to be

$$\begin{aligned} \hat{X}_{\delta\theta_Q, k, B}(n) &= -\frac{\epsilon\lambda}{2(\theta_k - \delta\theta_Q)\delta\theta_Q} \int_{-\infty}^{\infty} d\delta \sigma(\delta) \times \\ &\quad \left(\cos \left[n(\theta_k - \delta\theta_Q) - n\delta\theta_Q - \frac{\rho(\tau_B, \delta)}{\theta_s} \sin \varphi(\tau_B, \delta) \right] - \right. \\ &\quad \left. \cos \left[n(\theta_k - \delta\theta_Q) - \frac{\rho(\tau_B, \delta)}{\theta_s} \sin \varphi(\tau_B, \delta) \right] \right) \\ &= -\frac{\epsilon\lambda}{2(\theta_k - \delta\theta_Q)\delta\theta_Q} \left(\cos \left[n(\theta_k - \delta\theta_Q) - n\delta\theta_Q + \frac{\xi\omega_0\tau_B}{\eta} \right] - \right. \\ &\quad \left. \cos \left[n(\theta_k - \delta\theta_Q) + \frac{\xi\omega_0\tau_B}{\eta} \right] \right) \end{aligned} \quad (60)$$

which is independent of σ . If we define ψ to be the phase w.r.t. the kick $\epsilon\lambda \cos n\theta_k$, then it is easy to show that

$$\begin{aligned} \psi &= \tan^{-1} \left[\frac{\cos \left(\frac{3}{2}n\delta\theta_Q - \frac{\xi\omega_0\tau_B}{\eta} \right)}{\sin \left(\frac{3}{2}n\delta\theta_Q - \frac{\xi\omega_0\tau_B}{\eta} \right)} \right] - \pi \\ &= -\frac{\pi}{2} - \frac{3}{2}n\delta\theta_Q + \frac{\xi\omega_0\tau_B}{\eta} \end{aligned} \quad (61)$$

because $\cot \theta = \tan(\pi/2 - \theta)$ and the $-\pi$ is from the “-” sign in front of $\epsilon\lambda$. (61) makes

physical sense, because we expect $\psi = -\pi/2$ at resonance when $\tau_B = 0$. Now, from (61), we can immediately read off the phase difference $\psi(\xi, \tau_B)$ between the tail at $-\tau_B$ w.r.t. the head at $+\tau_B$ to be

$$\Delta\psi(\xi, \tau_B) = -\frac{2\xi\omega_0\tau_B}{\eta} \quad (62)$$

which is astonishingly simple for all the work that we have done! However, we must again remind ourselves that (62) is only valid if $\delta\theta_Q \ll \theta_s \ll 1$ or $\delta\theta_Q = 0$. The second case will be derived in *Case B*: $\theta_Q \approx \theta_s$.

Case A: Numerical Check

We will verify the formula (62) for two different $\delta\theta_Q$ for two different chromaticities with numerically calculated solutions. See Table 2. The first case is when $\delta\theta_Q = -0.5 \times 10^{-3}$ which in tune units is 8×10^{-5} below the betatron tune. The second case is when $\delta\theta_Q = -2\pi \times (0.5 \times 10^{-3})$ which is a more realistic 0.0005 tune units below the betatron tune. In both cases, $|\delta\theta_Q| < \theta_s/2$.

Table 2. Parameters used in the simulations

Parameter	Value	Parameter	Value
θ_Q	20.585	$\delta\theta_Q$	$\begin{cases} -0.5 \times 10^{-3} \\ -2\pi \times (0.5 \times 10^{-3}) \end{cases}$
θ_k	$\theta_Q + \delta\theta_Q$	θ_s	$2\pi \times (1.77 \times 10^{-3})$
ω_0	$2\pi \times (47.71 \times 10^3) \text{ s}^{-1}$	τ_B	$\pm 10^{-9} \text{ ns}$
ξ	3, 6	δ_B	1×10^{-4}
η	0.0028	ϵ	0.01
$y(0)$	0.0	$\dot{y}(0)$	0

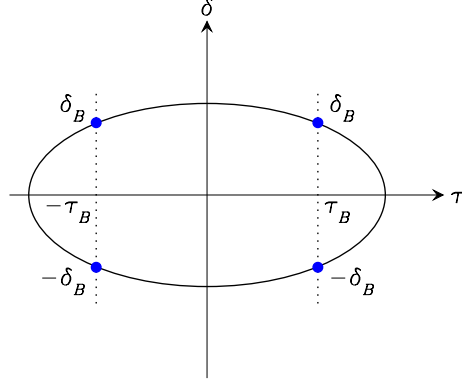


Figure 10 The σ distribution is an infinitely thin ellipse in the (τ, δ) plane which passes through $\pm(\tau_B, \delta_B)$.

Since (62) is independent of the δ distribution if σ is symmetric about $\delta = 0$, we choose σ to be the simplest possible distribution that matches to the RF bucket. See Figure 10. It is an infinitely thin ellipse that passes through the points $\pm(\tau_B, \delta_B)$. Therefore, we only need to average the transverse position over 2 points at (τ_B, δ_B) and at $(\tau_B, -\delta_B)$ to get the mean head position at τ_B . We perform a similar average for the tail at $-\tau_B$.

The expected phase difference using (62) is

$$\left. \begin{aligned} \Delta\psi(\xi = 3) &= -36.8^\circ \\ \Delta\psi(\xi = 6) &= -73.6^\circ \end{aligned} \right\} \quad (63)$$

These values are plotted in Figures 11 for the two different $\delta\theta_Q$ cases. It is evident from here that the closer we are to the betatron tune, the better the agreement between the numerically calculated phase difference and (62). There are phase jumps in the simulated phase difference which has a period of $2\pi/\delta\theta_Q$. This can be traced to the long period zeros of (60)

$$\Rightarrow \left. \begin{aligned} \cos \left[n(\theta_k - \delta\theta_Q) - n\delta\theta_Q + \frac{\xi\omega_0\tau_B}{\eta} \right] - \cos \left[n(\theta_k - \delta\theta_Q) + \frac{\xi\omega_0\tau_B}{\eta} \right] &= 0 \\ \sin \left[n(\theta_k - \frac{3}{2}\delta\theta_Q) + \frac{\xi\omega_0\tau_B}{\eta} \right] \sin \left[\frac{1}{2}n\delta\theta_Q \right] &= 0 \end{aligned} \right\} \quad (64)$$

Therefore, the long period between zeros is $2\pi/\delta\theta_Q$. See Figure 11.

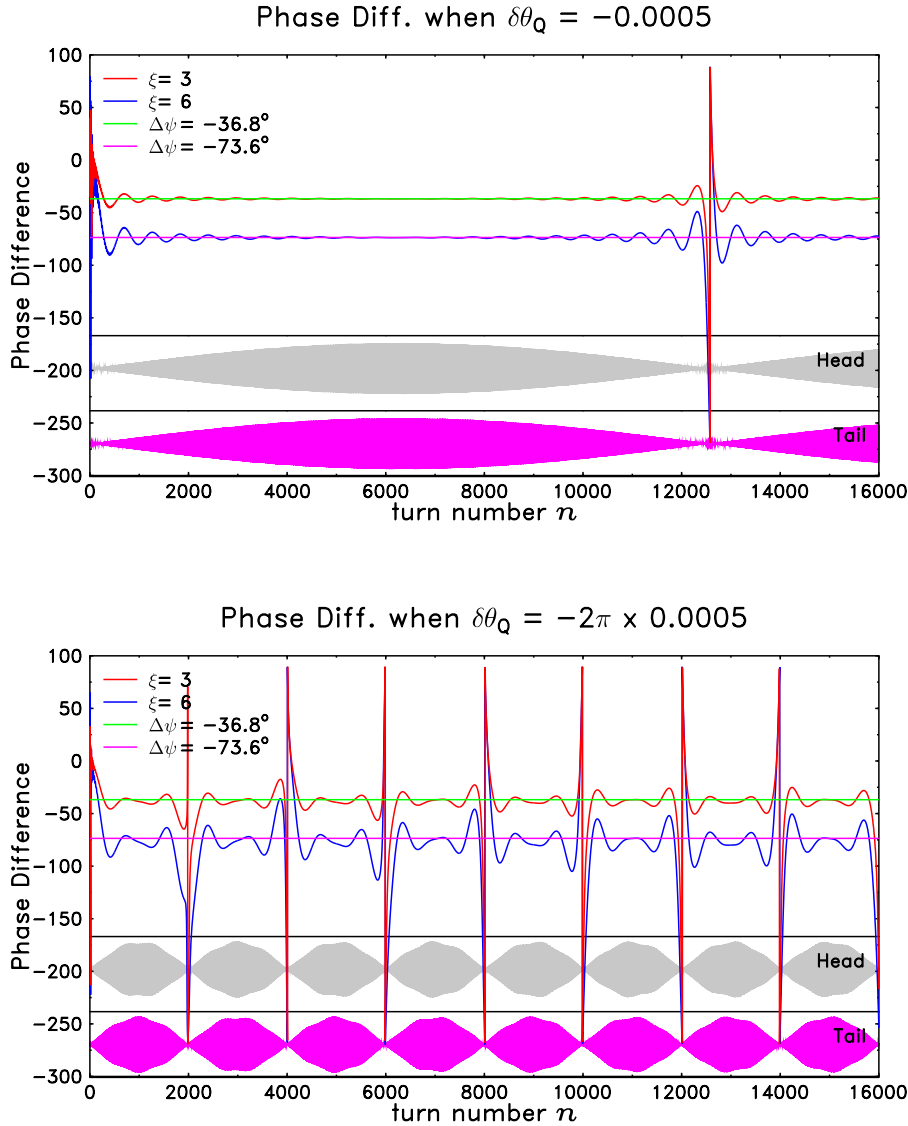


Figure 11 These figures show the numerically calculated phase difference between the tail w.r.t. head for two different $\delta\theta_Q$'s and two different ξ 's. We have superimposed the averaged positions of the head (grey) and tail (magenta) on this plot. The phase jumps come every $2\pi/\delta\theta_Q$ which coincides with the nodes of the head and tail positions.

Case B: $|\delta\theta_Q| \approx \theta_s$

In this case, the tune tracker PLL is locked to the closest synchrotron line w.r.t. the betatron tune. The relevant terms for this case from (53) are the ones with coefficients $1/(\delta\theta_Q - \theta_s)$. Instead of finding an analytic approximation, we will just numerically calculate the phase difference of the tail w.r.t. head for the case when $\delta\theta_Q = -0.01 \approx -\theta_s$ and $\xi = 3$. The distributions and parameters are those described in *Case A* and Table 2. The results are shown in Figure 12. It is clear that the phase difference does not match the simple formula (62) derived in *Case A*.

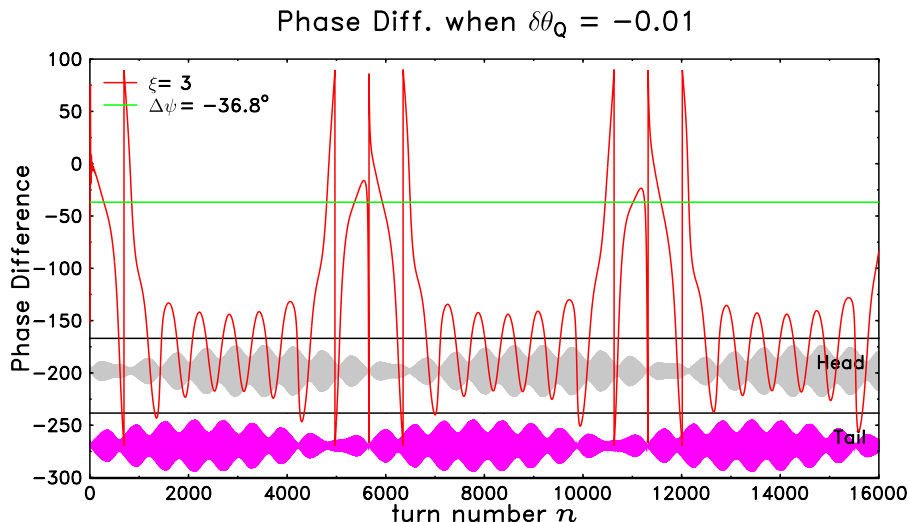


Figure 12 This plot shows the phase difference between the tail w.r.t. head for $\delta\theta_Q = -0.01$ and $\xi = 3$. The green line is at -36.8° calculated from (62) which clearly does not match what we numerically calculate.

This section shows that we have to be careful when we measure the chromaticity using the continuous headtail method. We have to make sure that the kick tune is close to the betatron tune and not on a synchrotron line.

Experiment

THE EXPERIMENT

In this experiment, the basic idea is for us to continuously kick the beam vertically with the AC-dipole. The phase difference between the head and tail due to this kick is then measured and plotted for different chromaticities.

Practically, we must first calibrate the knob T:CYINJ which we will use to change the vertical chromaticity. We do this by measuring the vertical chromaticity ξ_v for different T:CYINJ settings. The reason for using uncoalesced rather than coalesced beam is because it is much easier to measure chromaticity with uncoalesced beam with the traditional change of RF frequency method than with coalesced beam. The fit that we have found is

$$\xi_v = (0.78 \pm 0.03) \times \text{T:CYINJ} - (16.6 \pm 0.8) \quad (65)$$

From this fit, we find that the value of ξ_v when we are given T:CYINJ is approximately ± 0.65 units at a confidence level of 95% for the range of T:CYINJ that we will be setting. See Figure 13.

The experimental setup is shown in Figure 14.[†] We inject one coalesced bunch, which contains about 330×10^9 protons, to be used for the entire experiment. We set the chromaticity with T:CYINJ and then we kick the bunch transversely with the AC-dipole for a short period of time for each head tail phase measurement. The reason for turning off the AC-dipole is to keep the vertical emittance growth to a minimum. The exact ramp waveform of the AC-dipole is shown in Figure 14. The frequency of the kick is set to 0.6×10^{-3} tune units ($< Q_s = 1.7 \times 10^{-3}$) below the vertical betatron tune which is at 0.5776. The transverse position of the head and the tail are measured with a fast sampling oscilloscope and the phase difference is calculated offline. After each change of chromaticity,

[†] Note that there is no direct diode detector baseband tune (3D-BBQ) electronics in the setup so that there cannot be any arguments as to whether the phase difference effect is an artifact of the 3D-BBQ.

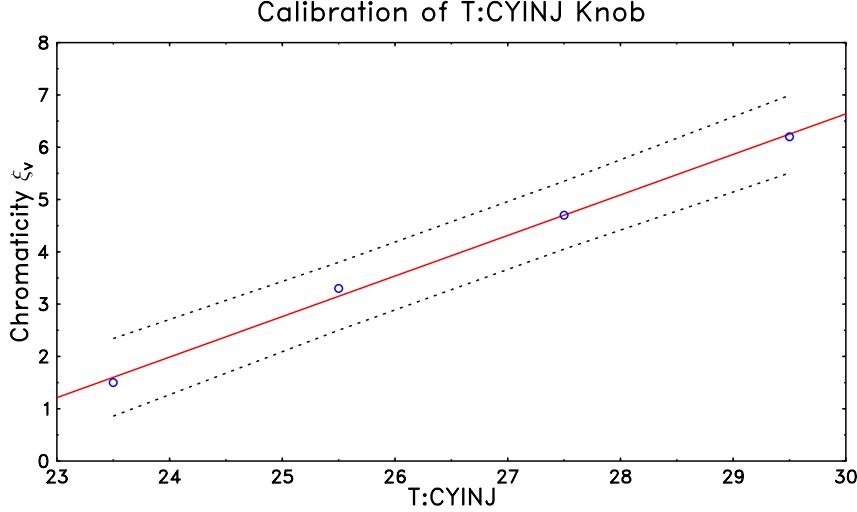


Figure 13 The T:CYINJ knob is calibrated with chromaticity measured with uncoalesced beam instead of coalesced beam. The dotted lines are the 95% confidence intervals.

we move the vertical tune if necessary to ensure that the betatron tune remains at 0.5776. Figure 15 shows some of the parameters we have collected during the experiment. Despite having set the AC-dipole kick to its minimum value, the vertical emittance T:PVEMIT, measured with the flying wires system, grows from 17π mm·mrad to 36π mm·mrad during the experiment. The sigma bunch length σ_B did not change during this time and is 2.9 ns.

Figure 16 shows an example of the head tail phase difference which we have analysed. In this example $\xi_v = 4$ and $\tau_B = 0.8$ ns. From here it is unambiguous that there is a phase difference between the head w.r.t. tail. (Note: in the data analysis, we present phase differences of the head w.r.t. tail rather than tail w.r.t. head used in the *Theory* section. This accounts for the sign difference.)

The measured phase difference $\Delta\psi$ for three values of $\tau_B = 0.4$ ns, 0.8 ns and 1.2 ns versus ξ_v are shown in Figure 17. The red line is the expected $\Delta\psi$ as a function of ξ_v from (62) where we have used the values ω_0 and η from Table 2. To check how good our

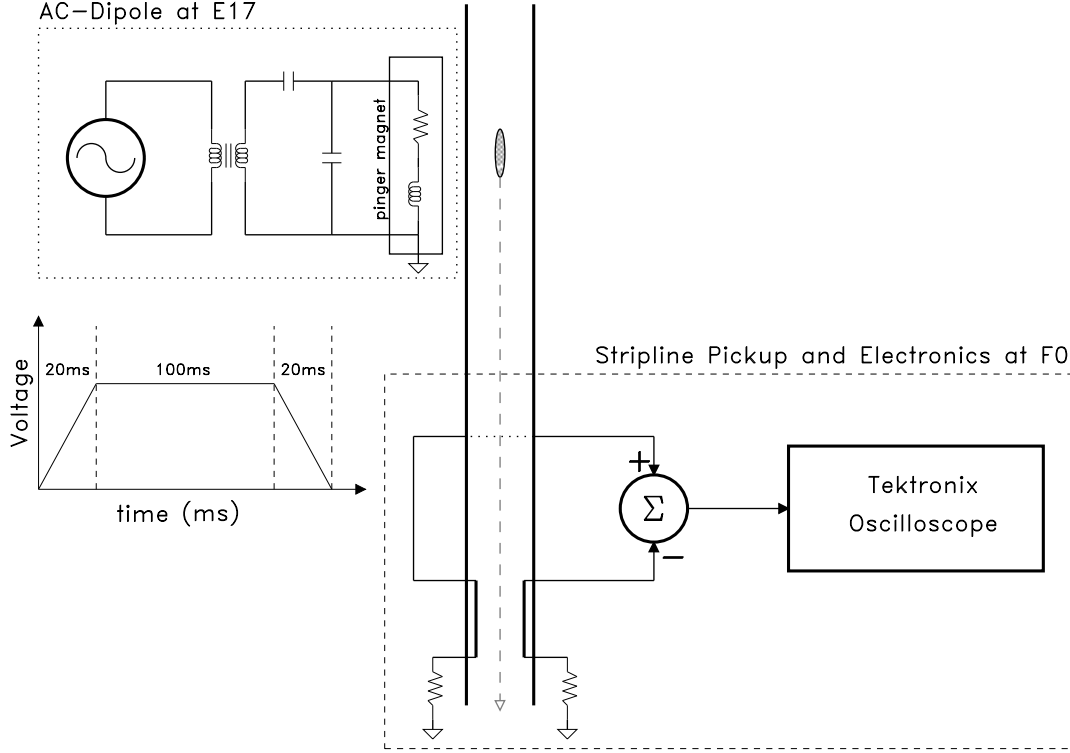


Figure 14 The experimental setup consists of an AC-dipole at E17 and a stripline with its electronics at F0. The AC-dipole is ramped up to its set voltage in 20 ms and stays at flattop for about 100 ms (equivalent to about 10 synchrotron periods or 5000 turns) and then ramped down again in 20 ms.

theory fits to the data despite the non-zero vertical emittance, we have calculated χ^2 and the reduced χ^2 for these three cases which are summarised in Table 3.

Table 3. χ^2 Comparison between Experiment and Theory

τ_B (ns)	τ_B/σ_B	χ^2	$P(\geq \chi^2)$	Reduced χ^2
0.4	0.14	5.8	0.67	0.72
0.8	0.28	9.6	0.29	1.2
1.2	0.41	8.8	0.35	1.1

For $\tau_B = 0.4$ ns, the probability that $\chi^2 \geq 5.8$ from pure chance is 0.67. This probability means that the data only matches the theory moderately well. The reduced $\chi^2 = 0.72$

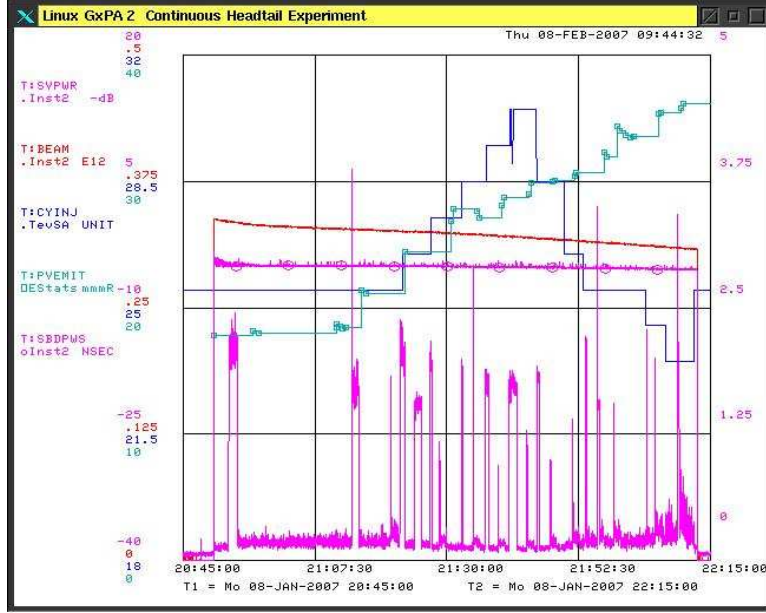


Figure 15 This figure shows some of the parameters that were measured during the entire experiment. T:CYINJ was changed and then the AC-dipole was fired. The Schottky power T:SVPWR spiked whenever the AC-dipole fired. The vertical emittance T:PVEMIT grew from 17π mm·mrad to 36π mm·mrad from the start to the end of the experiment. The beam intensity T:BEAM showed a lifetime that was similar to that of an undisturbed beam. The rms bunch length T:SBDPWS was 2.9 ns throughout the experiment.

is not that close to 1 which confirms that the match is not great. When we look at the red line in Figure 17(a) it is obvious that the χ^2 goodness of fit arguments are true.

For $\tau_B = 1.2$ ns and 2.4 ns, the probability that $\chi^2 \geq 9.6$ and 8.8 from pure chance are 0.29 and 0.35 respectively. From here, we can conclude that the data does not match the theory at all. Surprisingly, the reduced $\chi^2 \sim 1$ in both cases which means that the linear fits are reasonably good. This result is clearly misleading from examining Figure 17(b) and (c). It is obvious that that the theory does not fit the data for these two cases.

We suspect that there is a quadratic component ξ_v^2 that is not taken care of in the

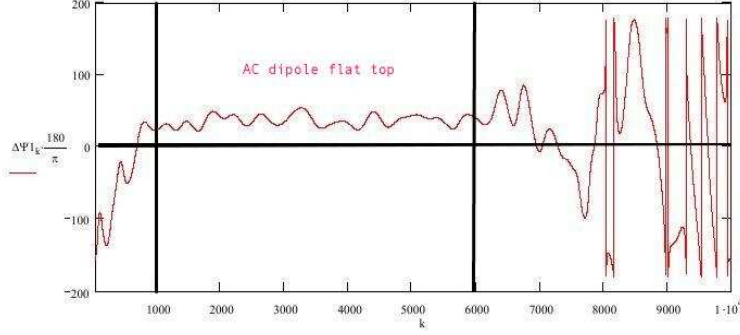


Figure 16 This shows the calculated phase difference between the head w.r.t. tail. This plot is for $\xi_v = 4$, $\tau_B = 0.8$ ns. The phase difference is $\Delta\psi = (30 \pm 7)^\circ$ during the 100 ms (5000 turns) flattop period of the AC-dipole kicker. See Figure 14. The ripples during this time gives us the error of the phase measurement.

theory. By fitting the data with

$$\Delta\psi = \xi_v(a\xi_v + b) \quad (66)$$

where a and b are fit parameters, we can explore how good this hypothesis is. The blue curves in Figure 17 show the quadratic fit and Table 4 shows the fit parameters.

Table 4. Quadratic Fit of Data

τ_B (ns)	τ_B/σ_B	a	b	Reduced χ^2
0.4	0.14	0.8 ± 0.1	1.6 ± 0.5	0.42
0.8	0.28	1.5 ± 0.3	3 ± 1	0.59
1.2	0.41	2.2 ± 0.4	4 ± 1	0.97

It is clear from the plots that the quadratic fits are rather good despite the wildly different reduced χ^2 for each case.

Sources of the Quadratic Term

There are several possible sources for the quadratic term ξ_v^2 . Equation (62) is derived

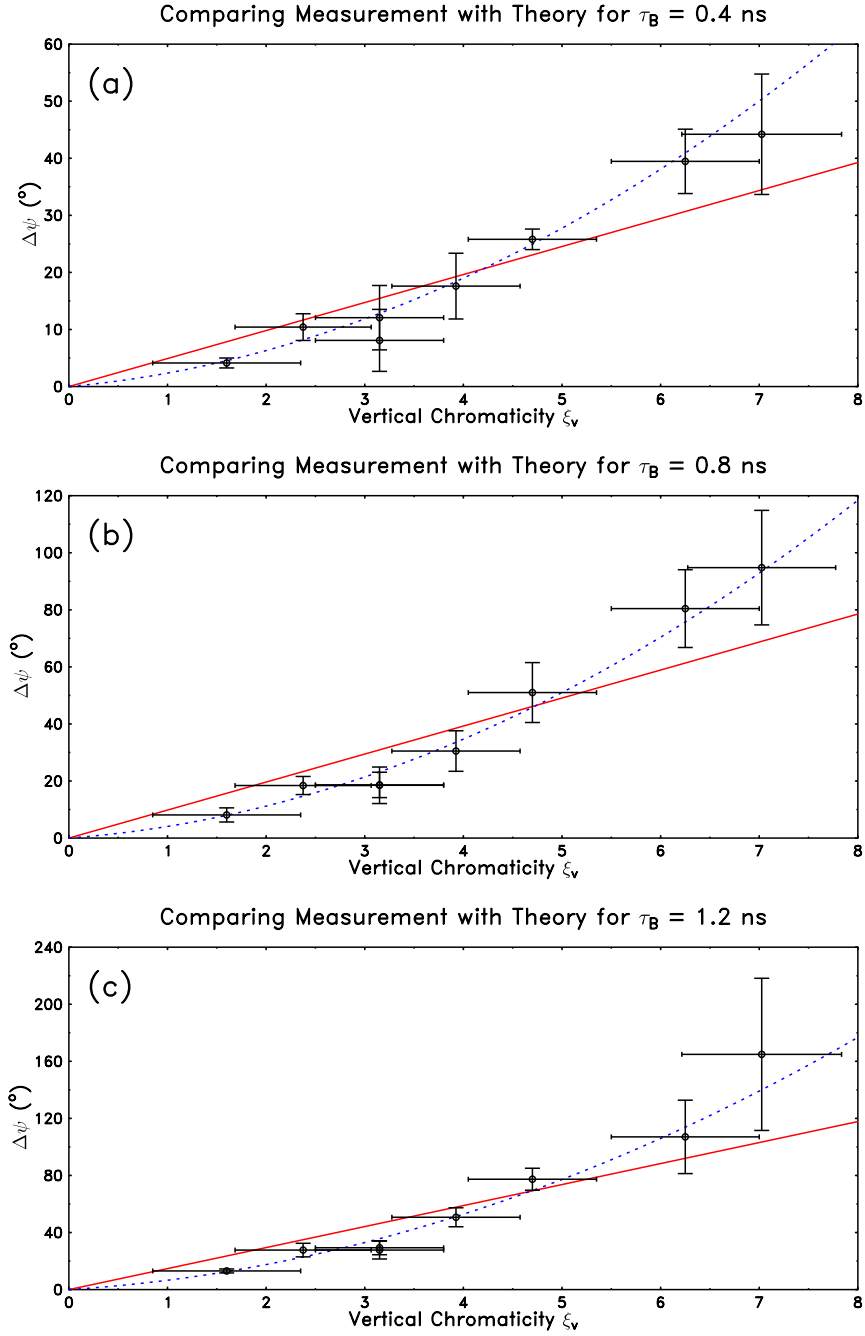


Figure 17 These plots show the data analysed for $\tau_B = 0.4$ ns, 0.8 ns and 1.2 ns. The red line is calculated from (62) and the blue dotted line is a quadratic fit of the data using coefficients from Table 4.

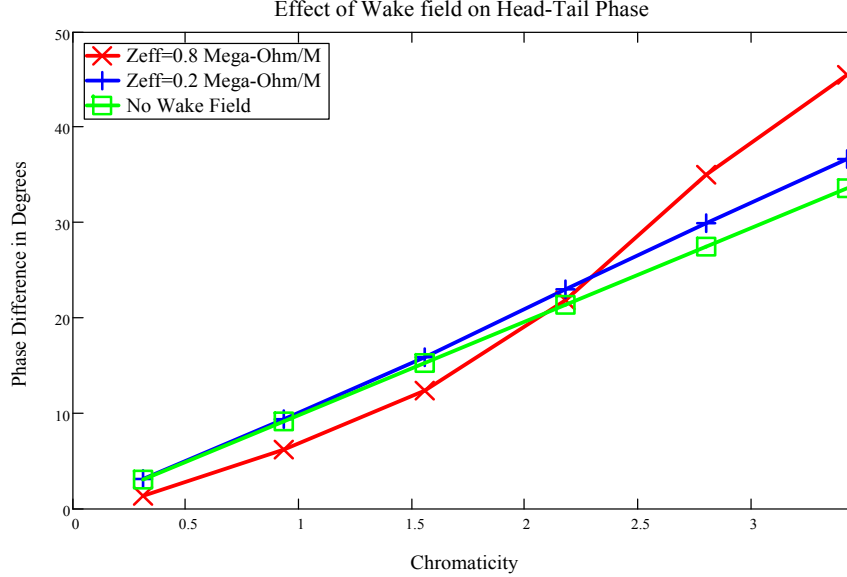


Figure 18 The effect of resistive wall wake field on the measured phase difference between the head slice (+0.4 ns from bucket center) and the tail slice (−0.4 ns from bucket centre) for a *single kick*. The red trace shows the effect of impedance at 0.8 MΩ/m, blue trace at 0.2 MΩ/m and the green trace is for zero impedance.

by assuming that the RF bucket is linear and that the transverse emittance is zero. Another possibility is that the transverse impedance is influencing the phase shift between the head and the tail. Whether these possibilities are the sources for the quadratic term will have to be resolved with computer simulations.

We do not think that second order chromaticity is the source of the quadratic term because they tend to cancel out when we take the difference between the head and the tail. The best candidate for the source of the quadratic term would seem to come from the impedance in the beam pipe. A more careful analysis of the effect of transverse impedance is provided using a multi-particle simulation driven by a *single kick*, which includes linear chromaticity and the effect of a short range resistive wall wake field. In Figure 18 we can see that the maximum phase difference as a function of chromaticity acquires a quadratic term as the strength of the wake field is increased.

Epilogue

CONCLUSION

We have mostly answered the questions that were asked at the end of *Introduction*. We have found an analytic approximation for the weakly forced Hill's equation which describes the transverse motion of the beam in the presence of chromaticity for a single particle. We have checked that our analytic approximation matches very closely to the numerically integrated solution. From here, we have derived an analytic approximation which shows that there is a phase difference between the head and tail for a zero transverse emittance but non-zero longitudinal length bunch. A simple formula for this phase difference has been derived when the kick tune is very close to the betatron tune. In this case, we have compared the analytically calculated phase difference to numerically calculated ones and we have shown them to be very close.

For the experiment, we have used the AC-dipole to excite the beam transversely and then measured the head-tail phase of the bunch. We have shown that there is a phase difference between the head and tail and thus have removed any lingering doubts as to whether the effect is real or not. From the measured data, we have found that there is a quadratic term which is not taken care of by the theory. Several possible sources, with short range wake fields being the best candidate, of this term have been proposed which we will have to resolve with computer simulations.

ACKNOWLEDGEMENTS

We would like to thank the following people:

- (i) A. Jansson and R. Miyamoto for helping us with the AC-dipole experiment.
- (ii) The run coordinator, B. Drendel, for giving us machine studies time to perform the experiment.
- (iii) Prof. Hoppensteadt for giving us his permission for quoting his book in *Appendix I*.

Appendices

APPENDIX I: THE NONLINEAR AVERAGING

The theorems, which we have copied here (with permission) in almost verbatim form from Hoppensteadt,¹⁰ are here for the reader's convenience.

The system of differential equations to be considered is

$$\frac{dx}{dt} = \epsilon f(t, \epsilon t, x, \epsilon) \quad (67)$$

or equivalently

$$\frac{dx}{d\tau} = f\left(\frac{\tau}{\epsilon}, \tau, x, \epsilon\right) \quad (68)$$

where $x, f \in E^n$, $|\epsilon| \ll 1$ and the slow time variable $\tau = \epsilon t$ is restricted to some finite interval $0 \leq \epsilon t \leq T < \infty$.

Hypothesis H1 $f(t, \tau, x, \epsilon)$ is a smooth function of its arguments for $0 \leq t \leq T/\epsilon$, $0 \leq \tau \leq T$, for x in some domain G lying in E^n , and for ϵ near zero. Moreover, suppose that f is an almost periodic function of t , uniformly in the other variables. Specifically, we assume that f can be expanded in a uniformly convergent generalized Fourier series

$$f(t, \tau, x, \epsilon) = f_0(\tau, x, \epsilon) + \sum_{n=1}^{\infty} f_n(\tau, x, \epsilon) e^{i\omega_n t} \quad (69)$$

where the frequencies ω_n satisfy $\omega_n \neq 0$ for $n \geq 1$.

Hypothesis H2 Let $g = f - f_0$, and suppose that the integral

$$\int_0^t g(t', \tau, x, 0) dt' = \int_0^t \left[f(t', \tau, x, 0) - \langle f \rangle(\tau, x, 0) \right] dt' \quad (70)$$

is bounded uniformly for $0 \leq t \leq T/\epsilon$ (and so for $0 \leq \tau \leq T$) and for $x \in G$.

The average of a function \bar{f} w.r.t. t is defined to be

$$\bar{f}(\tau, x, \epsilon) \equiv \lim_{T \rightarrow \infty} \frac{1}{T} \int_0^T \sum_{n=0}^{\infty} f_n e^{i\omega_n t} dt = f_0(\tau, x, \epsilon) \quad (71)$$

Nonlinear Averaging Theorem Suppose conditions H1 and H2 are satisfied and suppose that the averaged system

$$\frac{dX}{d\tau} = f_0(\tau, X, 0), \quad X(0) = \eta \quad (72)$$

has a unique solution lying in G for $0 \leq \tau \leq T$. If ϵ_0 is sufficiently small and if $|\epsilon| \leq \epsilon_0$, then:

1. There is a unique solution of the problem

$$\frac{dx}{dt} = \epsilon f(t, \epsilon t, x, \epsilon), \quad x(0) = \eta \quad (73)$$

for $0 \leq t \leq T/\epsilon$.

2. The solution lies in G .
3. There is a constant K depending on T and ϵ_0 such that

$$|x(t) - X(\epsilon t)| \leq K|\epsilon| \quad (74)$$

for $0 \leq t \leq T/\epsilon$.

This result shows that the solution of the averaged equation (72) approximates the solution of the full problem having the same initial data over large (growing) intervals, $0 \leq t \leq T/\epsilon$.

Now suppose that $T = \infty$ in conditions H1 and H2. Adding a stability condition can result in an approximation that is valid on the entire half-line $0 \leq t < \infty$. We say that the system is *mean stable* if condition H3 is true.

Hypothesis H3 The averaged equation

$$\frac{dX}{d\tau} = f_0(\tau, X, 0) \quad (75)$$

has a rest point, say X^* , that is exponentially asymptotically stable.

Averaging Theorem for Mean-Stable Systems Let f satisfy H1, H2 and H3.

Let X denote the solution of the initial value problem

$$\frac{dX}{d\tau} = f_0(\tau, X, 0), \quad X(0) = \eta \quad (76)$$

for $0 \leq \tau < \infty$. If η is near X^* and if $\epsilon > 0$ is sufficiently small, then the problem

$$\frac{dx}{dt} = \epsilon f(t, \epsilon t, x, \epsilon), \quad x(0) = \eta \quad (77)$$

has a unique solution for $0 \leq t < \infty$ and

$$x(t, \epsilon) = X(\epsilon t) + O(\epsilon) \quad (78)$$

where the error estimate here holds as $\epsilon \rightarrow 0^+$ uniformly for $0 \leq t < \infty$.

REFERENCES

- [1] S. Fartoukh & J.P. Koutchouk, *On the Measurement of the Tunes, Coupling & Detunings with Momentum and Amplitude in LHC*, LHC-B-ES-0004 rev 2.0.
- [2] C.Y. Tan, *Chromaticity: Measurement Techniques*, LARP Tune Feedback Review, http://www.agsrhichome.bnl.gov/LARP/061024_TF_FDR/talk_7_Tan_Chrom.pdf, 2006.
- [3] D. Cocq *et al*, *The Measurement of Chromaticity Via a Head-Tail Phase Shift*, <http://www.slac.stanford.edu/pubs/confproc/biw98/schmickler.pdf>, 1998.
- [4] P. Cameron, *Private Communication*, 2006.
- [5] V.I. Arnold, *Mathematical Methods of Classical Mechanics, 2nd Edition*, pg. 292, Springer-Verlag, 1989.
- [6] J.A. Sanders & F. Verhulst, *Averaging Methods in Nonlinear Dynamical Systems*, pg. 18, Springer-Verlag, 1985.
- [7] R.W. Brankin *et al*, RKSUITE Release 1.0, http://www.netlib.org/ode/rksuite/rksuite_90.zip, 1991.
- [8] A.W. Chao, *Physics of Collective Beam Instabilities in High Energy Accelerators*, pg. 218-233, John Wiley & Sons, 1993.
- [9] C.Y. Tan, *A Method for Calculating Longitudinal Phase Space Distribution when Given the Time Profile of the Bunch.*, TM-2155, 2001.
- [10] F.C. Hoppensteadt, *Analysis and Simulation of Chaotic Systems*, pg. 194-198, Springer-Verlag, 1993.